DEUTSCHES ELEKTRONEN – SYNCHROTRON DESY

DESY 89-075
June 1989

Perspectives on Physics at HERA

G.A. Schuler

II. Institut für Theoretische Physik, Universität Hamburg

ISSN 0418-9833

NOTKESTRASSE 85 · 2 HAMBURG 52

To be sure that your preprints are promptly included in the
HIGH ENERGY PHYSICS INDEX,
send them to the following address (if possible by air mail):

DESY
Bibliothek
Notkestrasse 85
2 Hamburg 52
Germany

DESY 89-075
June 1989

ISSN 0418-9833

PERSPECTIVES ON PHYSICS AT HERA [1]

G. A. Schuler
II. Institut für Theoretische Physik [2],
Universität Hamburg

Abstract

Physics opportunities at the *ep* collider HERA are reviewed. Possible tests of the Standard Model are outlined. Prospects of measurements of structure functions and tests of QCD are considered. Possibilities to search for new particles and interactions are surveyed. Perspectives on the determination of electroweak parameters in *ep* collisions are discussed.

[1] Expanded version of a talk presented at the Workshop on Results and Perspectives in Particle Physics, La Thuile, Italy, February 26 – March 4, 1989.

[2] Supported by Bundesministerium für Forschung und Technologie, 05 4HH 92P/3, Bonn, FGR.

1 Introduction

Deep inelastic lepton-nucleon scattering has been one of the key testing grounds in the development of the Standard Model (SM) in the past. Measurements of the nucleon and nuclear structure functions have not only tested the short-distance properties of QCD — such as scaling properties — but they have also illuminated the nonperturbative bound state structure of the nucleon and nuclei in terms of their quark and gluon degrees of freedom. In the electroweak sector fixed target lepton-nucleon experiments have provided one of the major quantitative tests of the Standard Model through measurements of the weak neutral (NC) and charged currents (CC). In fact, such experiments gave the first evidence, in 1961, for the separate identity of electron and muon neutrinos and for the existence of the weak neutral currents in 1973. The kinematic area that has been explored to date in lepton-nucleon scattering is Q^2 up to a few hundred GeV^2 and x above about 0.03. Similarly, photoproduction experiments have reached cms energies up to about 20 GeV.

HERA [1] presently under construction at DESY will be the first electron-proton collider. With the planned beam energies, E_e = 15–30 GeV and E_p = 300–820 GeV, cms energies between $\sqrt{s}$ = 134 GeV and $\sqrt{s}$ = 314 GeV will become available. The maximum possible momentum transfer is $Q^2_{max} = s \approx 10^5\,\mathrm{GeV}^2$. In practice, Q^2 is probably limited by the event statistics to $\sim 4 \cdot 10^4\,\mathrm{GeV}^2$. Thus HERA will extend the Q^2 range by a factor hundred. Also, due to the large cms energy the x-measurements can be greatly improved: even in the x-region between 10^{-4}–10^{-3} several million neutral current events are expected. Clearly, as for every collider, the physics potential of HERA will depend on its luminosity. The design luminosity is $\mathcal{L}$ = 1–$2\times10^{31}\,\mathrm{cm}^{-2}\mathrm{s}^{-1}$ leading to 100-200 pb^{-1} per year. This results e.g. in $O(10^7)$ NC and $O(10^4)$ CC events in a deep inelastic scattering (DIS) region defined by $Q^2 > 4\,\mathrm{GeV}^2$, $x > 10^{-3}$, and squared total hadronic energy $W^2 = (1-x)Q^2/x > 5\,\mathrm{GeV}^2$. Furthermore, both electron and positron beams will become available and a longitudinal lepton polarization of up to 80% is expected. Since $e^{\pm}_{L,R}$ all have different weak interactions with protons, the longitudinal polarization will greatly improve the possibility to disentangle different quark structure functions as well as to perform high precision measurements in the electroweak sector. The relevant experimental information will, for the most part, be obtained from inclusive measurements. Perspectives on tests of the SM at HERA will be discussed in the next sections.

Besides the deep inelastic regime HERA offers a wide variety of physics at low Q^2. Photoproduction cross sections are large and well measurable through forward electron detectors. The kinematical range of present day photoproduction experiments will be extended by an order of magnitude. Photoproduction cross sections obtain contributions from reactions involving the pointlike couplings of the photon to the partons in the proton, the anomalous photon component, the VDM component, and from diffractive reactions. Interesting physics includes the production of new heavy particles and the measurement of the photon's gluonic content.

Studies of the hadronic part of HERA events test both the perturbative and nonperturbative properties of QCD. In jet physics at high Q^2 one can investigate, for example, the theoretically challenging processes which are governed by two, a priori equal, mass scales, e.g. Q^2 and $p^2_\perp(QCD)$. The understanding of the hadronization of both the quark and target jets can be improved in lepton nucleon scattering. Further interesting topics are studies of exclusive channels and of the class of fully contained NC events where besides the scattered lepton and the current jet a leading proton is measured through a forward proton spectrometer. In section 2 a more detailed outline of physics opportunities at HERA is given. Section 3 collects

the relevant DIS cross section formulae. Both theoretical uncertainties and constraints arising from possible experimental limitations of the accessible kinematical region are discussed. The prospects to determine quark and gluon momentum distributions at HERA are reviewed in section 4 and 5. QCD analyses, i.e. measurements of the logarithmic scaling violation of DIS structure functions and the determination of Λ_{QCD} are the contents of section 6. Possibilities to search for new particles and to test for new interactions with ep collisions in the HERA energy range are surveyed in section 7. Finally, in section 8, perspectives on electroweak physics at HERA are detailed. Experimentation at HERA with the two experiments, H1 and ZEUS [2], is scheduled to begin in 1990. Its physics will provide a complementary programme to the physics presently available and being planned for the future at hadron colliders, e^+e^- machines and fixed target experiments.

2 Physics opportunities at HERA

To indicate the physics opportunities of HERA it is instructive to consider the various "modes" under which an ep collider can operate. The factorization formula

$$d\sigma(ep \to X) = \sum_{a,b} \int_0^1 dx_a \int_0^1 dx_b\, G_{a/e}(x_a, \mu_F^2)\, G_{b/p}(x_b, \mu_F^2)\, d\hat{\sigma}(ab \to X) \qquad (1)$$

has general validity for all hard reactions in electron-proton scattering. As usual, the kinematics of inclusive ep scattering is characterized by the ep centre-of-mass energy $\sqrt{s}$, $s = (p_e + P)^2$, the squared momentum transfer $Q^2 \equiv -q^2 = -(p_e - p_\ell)^2$, the Bjorken-variable $x = Q^2/2P \cdot q$, the variable $y \equiv P \cdot q / P \cdot p_e = Q^2/xs$ and the total hadronic energy W, $W^2 = (P+q)^2 = (1-x)ys$. In these definitions p_e, p_ℓ and P denote the four-momenta of the incoming and scattered lepton and the incoming proton, respectively. μ_F in eq. (1) is the factorization scale, typically of the order of the scale which governs the hard scattering process. The primary subprocess is deep inelastic electron-quark scattering, $eq \to eq$, either through neutral current (NC) or charged current (CC) exchange. This "DIS mode" produces one quark jet and one recoil lepton at high $p_\perp$. The scale in high Q^2 events is set by the $p_\perp$ of the scattered lepton, $\mu_F \sim p_\perp^{DIS} = \sqrt{(1-y)Q^2}$. The well known DIS cross section formula follows from eq. (1) with $a = e$, $G_{e/e}(x) = \delta(1-x)$, and $b = q, \bar{q}$. Due to the large $p_\perp$ in DIS reactions the kinematics can be reconstructed with high accuracy from the hadron and/or lepton side so that this mode is ideal for precision tests of the SM. These include first of all measurements of the shape in Bjorken-x of the structure functions, $F_i(x, Q^2)$, and of the quark and gluon densities, but also more detailed tests like the scaling violation of the DIS structure functions, and the determination of the running coupling constant, $\alpha_s(Q^2)$, and therefore of Λ_{QCD}. Also, tests of the electroweak sector of the SM are best performed in this mode. These inlude the structure of the weak and charged weak currents, the Z and W propagators as well as real boson production, electroweak radiative effectcs and of extensions of the SM.

The "low-Q^2 mode" (photoproduction) corresponds to the sacttering of an almost real photon on the proton. It is the ideal testing ground of the hadronic nature of the photon and its structure functions. Photoproduction yields the largest cross sections of all ep processes. With help of the Weizsäcker-Williams approximation

$$\sigma_{ep}(s) = \int dy\, G_{\gamma/e}(y)\, \sigma_{\gamma p}(ys) \qquad (2)$$

where

$$G_{\gamma/e}(y) = \frac{\alpha}{\pi} \frac{1+(1-y)^2}{y} \ln\left(\frac{Q_{max}}{Q_{min}}\right) \tag{3}$$

one can relate photoproduction cross sections to the corresponding ones for electroproduction. The bounds on y and Q^2 depend on the kinematics of the reaction. Outside these bounds the cross section $\sigma_{\gamma p}$ becomes negligible. Taking $Q_{min} = m_e$, $Q_{max} = 1\,\mathrm{GeV}$ and $\ln(1/y_{min}) = 3$, $y_{max} = 1$, the untagged photon-proton luminosity can be estimated [3]

$$\mathcal{L}_{\gamma p} \approx 0.1 \cdot \mathcal{L}_{ep} \tag{4}$$

Tagging of electrons reduces the event rate, but allows more detailed studies since the variables (y, Q^2) can be measured. An example is the extraction of the gluon density from J/Ψ production at low Q^2. A tagger of photoproduction events is e.g. provided by the luminosity detectors. Virtual photons of energy $E_\gamma = E - E'$ can be tagged by measurement of the energy E' and the emission angle θ_e of the scattered electrons and consequently y and Q^2 can be evaluated according to the relation $y \approx 1 - E'/E$, $Q^2 \approx EE'\theta_e^2$ which is valid for $\theta_e \to 0$. For example, at ZEUS, the electron can be measured in the range $13 \leq E' \leq 23\,\mathrm{GeV}$ and $0 \leq \theta_e \leq 6\,\mathrm{mrad}$ [4]. Thus the accessible range is [3]

$$\text{poor tag:} \quad 1.7 \times 10^{-8} \approx \frac{m_e^2 y^2}{1-y} \leq Q^2 \leq 2.5 \times 10^{-2}\,\mathrm{GeV}^2 \quad , \quad 0.23 \leq y \leq 0.57 \tag{5}$$

$$\text{with an average acceptance off} \approx 70\%\,.$$

The overwhelming majority of tagged electrons will originate from bremsstrahlung (about a factor $\sim 3 \times 10^4$ larger). The requirement, $\theta_e \geq 1\,\mathrm{mrad}$, suppresses this bremsstrahlung background almost completely. Also, a precise measurement of the scattering angle is only possible for polar angles above 1 mrad. This defines the region

$$\text{golden tag:} \quad 3.9 \times 10^{-4} \leq Q^2 \leq 2.5 \times 10^{-2}\,\mathrm{GeV}^2 \quad , \quad 0.23 \leq y \leq 0.57 \tag{6}$$

$$\text{with an average acceptance of} \approx 20\%\,.$$

The interest in using an ep collider for studying low Q^2 processes derives from the large cms energies that can be obtained in the γp system. The photon-proton cms energy reachable at HERA is quite impressive, $150 \leq \sqrt{s(\gamma p)} \leq 240\,\mathrm{GeV}$. It corresponds to an equivalent laboratory energy in fixed target γp experiments of $12000 \leq E_\gamma^{Lab} \leq 30000\,\mathrm{GeV}$! The luminosities corresponding to poor and golden tag are:

$$\begin{aligned} \mathcal{L}_{\gamma p}(\text{poor tag}) &\approx 0.01 \mathcal{L}_{ep} \\ \mathcal{L}_{\gamma p}(\text{golden tag}) &\approx 0.001 \mathcal{L}_{ep} \end{aligned} \tag{7}$$

Hence a reaction with $1\mu b$ cross section will yield of the order of 10^6 events per year for the poor tag case and 10^5 with a golden tag. Contributions to the photoproduction cross section come from reactions where the photon couples pointlike to the partons in the proton and from subprocesses involving the photon structure function.

Subprocesses based on the pointlike coupling of the photon to the partons within the proton are QCD compton, $\gamma^* q \to gq$, and photon-gluon fusion, $\gamma g \to q\bar{q}$. They lead to two-jet production. These pointlike low Q^2 subprocesses dominate reactions in which the large transvers momentum trigger is a hadron rather than the scattered lepton as in the DIS mode: $\mu_F \sim p_\perp^{QCD}$. Since the photon propagator rises as $1/Q^2$ at low Q^2, see eq. (3), this "pointlike photon mode"

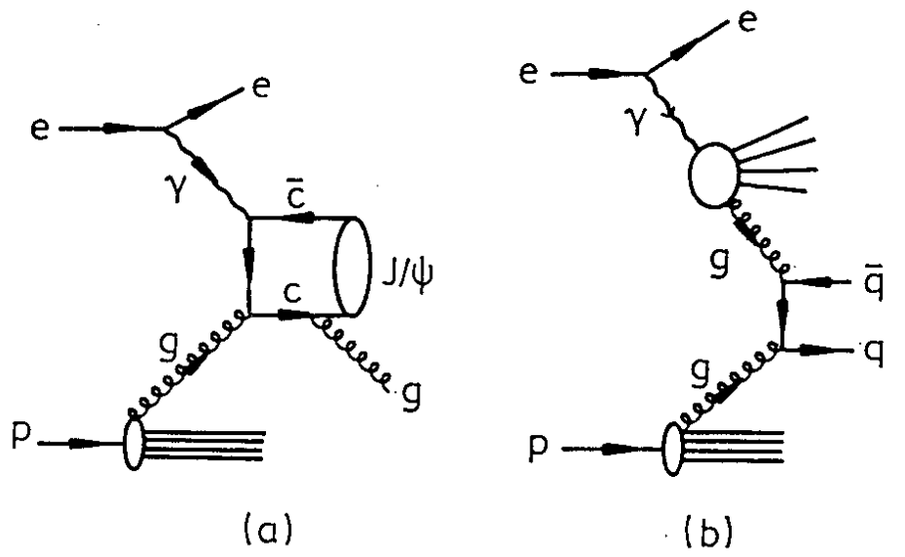

Figure 1: *(a) Generic Feynman diagram of J/Ψ production in ep collisions via photon-gluon fusion. (b) A typical process of the anomalous (or resolved) photon contributions to the photoproduction of hadrons.*

yields cross sections much larger than the DIS mode at fixed hadronic energy W and is thus the dominating source for the production of heavy objects at HERA. For example, heavy quark production proceeds dominantly via the reaction $\gamma g \to Q\bar{Q}$ [5]. Only for very heavy quark masses (a top quark above ≈ 55 GeV) single quark production via CC reactions dominates. Besides heavy flavour production also other heavy particles like the W and Z bosons are produced at low Q^2. Furthermore, the pointlike coupling component of the photon gives rise to single particle production, e.g. $\gamma + g \to J/\Psi + g$ shown in Figure 1a, to prompt photon production, and to the production of high $p_\perp$ jets. All these hard processes involving the pointlike coupling of the photon are described by eq. (1) with $a = \gamma$ and $b = q, \bar{q}, g$. In such a process the pointlike coupling of the photon to the proton's constituents directly probes the parton densities, and can give complementary information to the usual deep inelastic structure function methods.

Photoproduction also probes the hadronic nature of the photon. The processes are described by the photon structure function which is given by the sum of a VDM component and of an anomalous (resolved photon) component, see e.g. [6]:

$$G_{a/\gamma}(x, \mu_F^2) = G_{a/\gamma}^{VDM}(x, \mu_F^2) + G_{a/\gamma}^{AN}(x, \mu_F^2) \tag{8}$$

The anomalous component, proportional to $\ln(\mu_F^2/\Lambda^2)$, is calculable in perturbative QCD and gives rise to $q\bar{q}$, qg and gg initial states where the colliding partons are collinear. A typical process is shown in Figure 1b. Then electron-proton scattering behaves like a hadronic collider ("collider mode"). The cross sections are again described by eq. (1), now taking $a, b = q, \bar{q}, g$ and e.g.

$$G_{q/e}(x, \mu_F^2) = \int_x^1 \frac{dz}{z} G_{\gamma/e}(z)\, G_{q/\gamma}\left(\frac{x}{z}, \mu_F^2\right) \tag{9}$$

There is a wide variety of processes initiated by parton-parton scatterings like QCD processes (high $p_\perp$ jet production, minijets), production of heavy objects, prompt photon and lepton pair

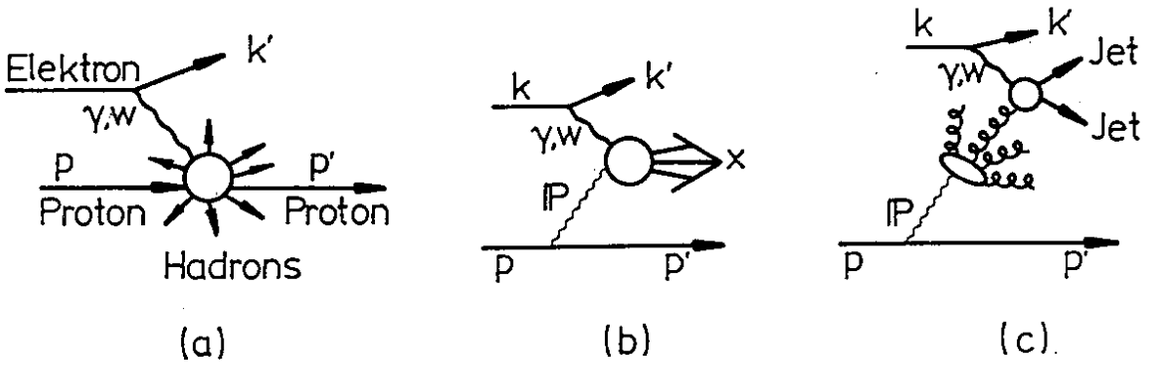

Figure 2: *(a) Diffractive production of a central hadronic system in ep scattering. (b) A hard diffractive interaction generated by pomeron exchange. (c) A model of the production of high $p_\perp$ jets in diffractive reactions.*

production, and the production of vector mesons, e.g. $\gamma p \to ggX \to \eta_c X$. In many of these processes the anomalous photon structure function should clearly be observable, see e.g. [6] for the case of π^0 photoproduction. In particular, HERA offers the possibility to explore the gluon distribution inside the photon $G_{g/\gamma}$, Figure 1b, which is not directly accessible in $\gamma\gamma^*$ experiments.

The VDM contribution in eq. (8) may be estimated as follows:

$$E\frac{d\sigma^{VDM}}{d\vec{p}}(\gamma p \to \gamma X) \approx \frac{1}{200} E\frac{d\sigma^{VDM}}{d\vec{p}}(\rho^0 p \to \gamma X) \tag{10}$$

The total photon-proton cross section can be estimated this way:

$$\sigma_{tot}(\gamma p) \approx 130\,\mu\text{b} \tag{11}$$

Among the reactions (10) leaving the proton intact are elastic Compton scattering, $\gamma p \to \gamma p$, and diffractive production of vector mesons. These processes can be studied at HERA. The ZEUS detector, for example, has a geometrical efficiency for the detection of fast forward protons which rises to a maximum of 60% for $x_F = 0.9$, falling to 30% at $x_F = 1.0$. Of particular interest are hard QCD scatterings in diffractive reactions at HERA. One expects to observe events in which the proton emerges almost undeflected and isolated in rapidity, and in which there is evidence from the central detector for a large momentum transfer process. A central cluster X of hadrons is produced as shown in Figure 2a. At HERA one can study diffractive central clusters with a mass M_X up to 100 GeV [8], which is nearly twice as much as the cms energy at the ISR. The whole variety of hard QCD scatterings, jets, heavy flavour production, etc., is expected to take place. These processes can be described by the exchange of a pomeron which then participates in a hard scattering, see Figure 2b. Hard diffractive processes [7], therefore, are a device to resolve the partonic structure of the pomeron. Essentially there are two descriptions of the structure of the pomeron, one assuming the pomeron to couple to quarks and gluons like an isoscalar $C = +1$ photon, Figure 2b, and one where the pomeron is mainly composed of gluons, Figure 2c. In the latter approach one can imagine the processes as being mainly initiated by photon-gluon fusion where the gluon originates from a pomeron which in turn is emitted by the proton. These hard reactions can therefore also be described by eq. (1)

with $a = \gamma$ and $G_{g/p}(x) = \int dz/z\, G_{pomeron/p}(z)\, G_{g/pomeron}(x/z)$. Using this description, it was shown in [8] that hard diffractive processes processes give non negligible contributions to the production of high $p_\perp$ jets and heavy flavours. Thus HERA will provide new insight into this aspect of QCD.

The different modes of ep scattering partly overlap. It is thus important to study their interrelations and to obtain a smooth matching of the models describing the various modes. As an example consider the interrelation of the DIS picture with the low Q^2 pointlike processes in more detail. The tree level DIS reaction is the quark-parton model $eq \to eq$ scattering whose description is valid for Q^2 above a few GeV^2. The tree level diagrams for low Q^2 processes are the $O(\alpha_s)$ reactions $\gamma q \to qg$ and $\gamma g \to q\bar{q}$. Here Q^2 can extend to extremely low values, $Q^2 \geq m_e^2(\hat{s}/s)^2 \sim 10^{-14}\,\mathrm{GeV}^2$. Now it is exactly these processes which make the $O(\alpha_s)$ corrections to the QPM scattering. Though DIS scattering occurs at high Q^2, there is a region where theses $O(\alpha_s)$ processes contribute to both pictures. Thus there is the potential problem of double counting certain contributions. A solution where one simply introduces a cut to separate different contributions runs into the problem of how to match smoothly the individual contributions. Closely related is the problem of scales. As long as the final state is unresolved, there is just one scale, namely Q^2. However, the production of high $p_\perp$ jets in DIS is governed by two scales, Q^2 and W^2, which can be of same size. Reactions involving two scales are a still largely unexplored phenomenon and their study is a challenge of ep scattering.

Another interesting task is the reconstruction of the final state in electroproduction. It will improve our understanding of the final state hadronization of both the quark and proton spectator jets. According to QCD factorization, the recoiling quark jet, together with the gluonic radiation produced in the scattering process, produces hadrons in a universal way, independent of the target or particular hard scattering. In contrast, the hadronization of the spectator system depends in detail on the target properties. Unlike the quark jet, the leading particles of the target spectator system do not evolve and thus should not depend on the momentum transfer Q^2 (at fixed W^2). While in most ep events the proton remnants are lost in the beam pipe it is possible to obtain information for a class of events which contains a leading proton via the forward proton detector of ZEUS. Protons with $x_L > 0.3$ can be detected with a momentum resolution of $\sigma(p)/p \sim 1\%$. As is well known the features of the standard leading twist description of lepton-nucleon scattering are modified by coherent or nonperturbative effects at low Q^2. Experimentation at HERA might help to clarify the distinction between logarithmic and power-law scale breaking effects and the effect of higher-twist contributions to ep cross sections. The interrelations between the various modes described above (diffractive processes, vector meson dominance, anomalous photon contributions, pointlike photon coupling contributions), Regge behavior in non-singlet structure functions, and other phenomena at the boundary between perturbative and non-perturbative effects — like jet-coalescense [9], intrinsic charm [10], etc. — are further topics that can be studied in ep scattering.

3 DIS cross sections

The fundamental quantities for precision measurements of the SM in DIS are the inclusive differential cross sections, $d^2\sigma/dxdQ^2$, for charged and neutral current interations of electron and proton beams. In the lowest order of the electroweak couplings and leading order QCD the

differential cross sections for NC scattering, $e^{\mp}p \to e^{\mp}X$, can be written as

$$\begin{aligned} \frac{d^2\sigma^{NC}(e^{\mp}p)}{dxdy} &= \frac{2\pi\alpha^2}{xyQ^2} Y_+ \tilde{\sigma}_{NC}(e^{\mp}) \\ \tilde{\sigma}_{NC}(e^{\mp}) &\equiv F_2(x,Q^2) \pm \frac{Y_-}{Y_+} x F_3(x,Q^2) \end{aligned} \tag{12}$$

The structure function F_1 has been eliminated through the Callan-Gross relation, $2xF_1 = F_2$. The quantities $Y_\pm$ are defined by: $Y_\pm = 1 \pm (1-y)^2$, and the quantity α in eq. (12) is the electromagnetic finestructure constant.

Effects of a nonzero proton mass and of primordial transverse momenta of the partons as well as higher twist operators can safely be neglected taking $Q^2 \geq 100$ GeV^2. Contributions of this kind are suppressed by inverse powers of Q^2. Also, thresholds from heavy quarks do not play a role in contrast to fixed target experiments. It has been shown that, at $Q^2 \geq 100$ GeV^2 and $x \geq 0.01$, contributions from $c\bar{c}$ production have a leading-logarithmic behaviour similar to that of light quarks, while contaminations from $b\bar{b}$, $t\bar{t}$ and presumably also from $t\bar{b}$ production are negligible [11]. Therefore, it is justified to take four massless quark flavours (u, d, s, c).

Using the above approximations the NC structure functions, $F_i(x,Q^2)$, can be expressed in terms of the quark and antiquark (number) density distributions $q_f(x,Q^2)$ and $\bar{q}_f(x,Q^2)$:

$$\begin{aligned} F_2(x,Q^2) &= \sum_{f=1}^{n_f} A_f(Q^2)\, x\, [q_f(x,Q^2) + \bar{q}_f(x,Q^2)] \\ x\,F_3(x,Q^2) &= \sum_{f=1}^{n_f} B_f(Q^2)\, x\, [q_f(x,Q^2) - \bar{q}_f(x,Q^2)] \end{aligned} \tag{13}$$

The electroweak coupling coefficients A_f and B_f depend on Q^2 and the lepton polarization, λ, ($+\lambda$ for e^+p and $-\lambda$ for e^-p scattering), and are different for up and down like quarks

$$\begin{aligned} A_f(Q^2) &= e_f^2 - 2e_f v_f \mathrm{Re}(\chi_Z)(v_e \pm \lambda a_e) + (v_f^2 + a_f^2) \mid \chi_Z \mid^2 (v_e^2 + a_e^2 \pm 2v_e a_e \lambda) \\ B_f(Q^2) &= -2e_f a_f \mathrm{Re}(\chi_Z)(a_e \pm v_e \lambda) + 2v_f a_f \mid \chi_Z \mid^2 \left(2v_e a_e \pm \lambda(v_e^2 + a_e^2)\right) \end{aligned} \tag{14}$$

Here χ_Z is the Z propagator

$$\chi_Z(Q^2) = \frac{1}{(2\sin 2\theta_W)^2} \frac{Q^2}{Q^2 + M_Z^2 - iM_Z\Gamma_Z} \tag{15}$$

and the electroweak couplings are given by $v_e = -1 + 4\sin^2\theta_W$, $a_e = -1$, $v_f = 2t_f - 4e_f \sin^2\theta_W$ and $a_f = 2t_f$ with the convention $e_u = +2/3, t_u = +1/2$, etc.

Using the unitary relations of the CKM matrix and restricting again to four massless quark flavours the differential cross section for CC interactions, $e^{\mp}p \to \nu_e(\bar{\nu}_e)X$, is given by

$$\begin{aligned} \frac{d^2\sigma^{CC}(e^{\mp}p)}{dxdy} &= \frac{xs\,(1 \mp \lambda)\pi\alpha^2}{4\sin^4\theta_W (Q^2 + M_W^2)^2} \tilde{\sigma}_{CC}(e^{\mp}) \\ \tilde{\sigma}_{CC}(e^-) &= u(x,Q^2) + c(x,Q^2) + (1-y)^2 \left[\bar{d}(x,Q^2) + \bar{s}(x,Q^2)\right] \\ \tilde{\sigma}_{CC}(e^+) &= \bar{u}(x,Q^2) + \bar{c}(x,Q^2) + (1-y)^2 \left[d(x,Q^2) + s(x,Q^2)\right] \end{aligned} \tag{16}$$

The quark distributions introduced above obey the Altarelli-Parisi evolution equations of QCD in the leading-logarithmic (LL) approximation [12].

The dominating next-to-leading-log (NLL) QCD corrections arise from a non-vanishing longitudinal structure function, $F_L \equiv F_2 - 2xF_1$, which in $O(\alpha_s)$ is given by:

$$F_L(x,Q^2) = C_F \frac{\alpha_s}{\pi} \int_x^1 \frac{d\eta}{\eta} \left(\frac{x}{\eta}\right)^2 \left\{ F_2(\eta,Q^2) + \left(\sum_{f=1}^{n_f} A_f(Q^2)\right) \frac{4T_R}{C_F} \left(1-\frac{x}{\eta}\right) \eta G(\eta,Q^2) \right\} \tag{17}$$

Here $G(x,Q^2)$ is the gluon number density distribution, $C_F = 4/3$, and $T_R = 1/2$. F_L can be approximated at small x by

$$F_L(x,Q^2) \approx \frac{\alpha_s}{\pi} \left(4T_R \sum_f A_f(Q^2)\right) \int_x^1 \frac{d\eta}{\eta} \left(\frac{x}{\eta}\right)^2 \left(1-\frac{x}{\eta}\right) \eta G(\eta,Q^2) \tag{18}$$

The effect of NLL terms reaches a few percent at small x and large Q^2 (or large y), and exceeds 10% at $x \leq 0.01$ and $y \geq 0.8$ [13]. This behaviour has its origin in the important contribution of the gluon density, see eq. (18). It can be kept small either by avoiding the small x and large Q^2 ranges or by averaging over suitable ranges in y. Then the resulting structure functions and quark densities are only shifted insignificantly and, as far as QCD is concerned, the LL approximation is certainly sufficient for most purposes.

In contrast, higher order electroweak corrections, particularly the electromagnetic radiative effects, are sizeable and must be taken into account. Complete one-loop calculations have been performed by different groups and, although some differences are still being discussed, there is a general consensus on the results [14]. For a phenomenological study not investigating higher order electroweak effects it is then convenient to assume that the analysis is applied to data that have been corrected for the electroweak radiative effects.

Compared to present day fixed target experiments a series of new features appears in the cross sections formulae (12–16) of high energy ep collisions. The effect of the rising strength of the weak neutral current interactions with increasing Q^2 is twofold. First, a new structure function, xF_3, appears in the cross-sections for $ep \to eX$. Secondly, the F_2 structure function deviates from the familiar expression valid at present-day energies

$$F_2^{em}(x,Q^2) = \sum_{f=u,d,s,c} e_f^2 \left[x q_f(x,Q^2) + x\bar{q}_f(x,Q^2)\right] \tag{19}$$

Moreover, the Z boson propagator, eq. (15), induces scaling violations by powers of Q^2/m_Z^2 which cannot simply be factored out, in contrast to the W propagator which enters the CC cross-section as an overall factor. In the upper Q^2 region accessible at HERA energies, these scale dependences become much stronger than the logarithmic scaling violations predicted by QCD, and therefore complicate QCD tests as discussed in refs. [15,16]. Also, the shape in x of structure functions averaged over y or Q^2 is affected. As a consequence, one must be quite careful when comparing measurements from future ep collider experiments with existing (low-Q^2) data.

Measurements of the structure functions and of the electroweak sector are based on the inclusive NC and CC cross sections differential in x and y or Q^2. The precision of these measurements is largely determined by the accuracy of the kinematics reconstruction and the

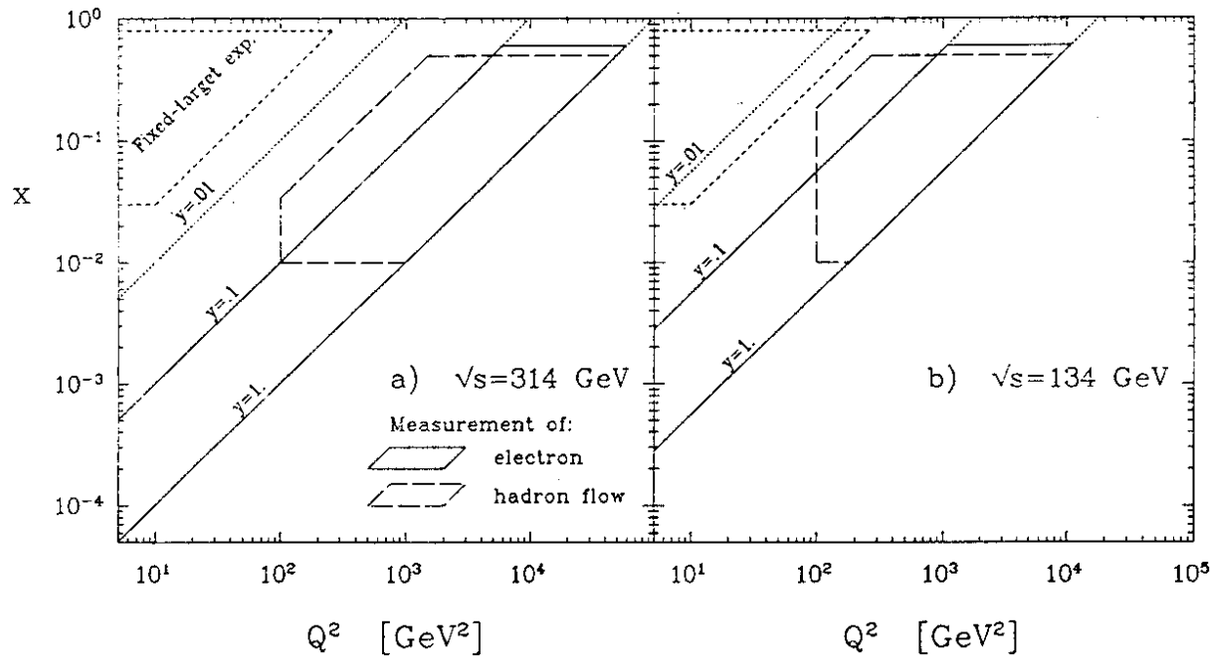

Figure 3: *Domains where systematic errors are below 10% for electron measurement (full line) and hadron flow measurement (dashed line). From ref. [18].*

quality of the NC/CC separation. While the kinematical variables can only be reconstructed from the hadronic system in CC events, they can also be measured from the scattered electron in NC events. The kinematics is obtained in bins of (x, Q^2) (or (x, y)) with sizes suitably chosen with respect to the available event statistics. The problems of event classification and kinematics reconstruction give rise to impure samples and migrations of events between different bins.

Signatures for NC/CC event separation are related to the appearance of a scattered electron in the NC case and an undetected neutrino in the CC case. Due to the escaping neutrino CC events are unbalanced in transverse momentum and deposit a smaller total energy in the calorimeter. In [17] it was shown that criteria based on the total energy, missing transverse momentum, and searches for an isolated lepton allow a very clean separation. Thus losses and contamination due to imperfect NC/CC separation are quite small and can usually be neglected.

The dominating source of errors in the cross section measurements are related to migrations due to erroneously measured event kinematics. The main limiting factors are calibrations of energies and, in the forward direction, granularity and the beam hole of the hadronic calorimeters. The resulting shifts in the kinematical variables can only partly be corrected for. A useful region can be defined by the requirement that the smeared acceptance is close to one. These problems are investigated in detail in [18]. Assuming a minimum scattering angle of about 4° for the electron measurement and requiring a $p_\perp > 10\,\mathrm{GeV}$ for the jet the following domains were found where the systematic errors can be kept below 10%:

$$\begin{aligned} \text{electron measurement} &: 5 \times 10^{-5} < x < 0.6 \;,\; Q^2 > 5\,\mathrm{GeV}^2 \;,\; y > 0.1 \\ \text{hadron measurement} &: 0.01 < x < 0.5 \;,\; Q^2 > 100\,\mathrm{GeV}^2 \;,\; y > 0.03 \end{aligned} \tag{20}$$

The accessible regions are shown in Figure 3. If analyses of structure functions and electroweak

studies are restricted to the above defined safe regions, then the systematic errors on the differential cross sections are usually small compared to the statistical errors and can be negelected, at least to a first approximation. At 200 pb^{-1} one can expect the following number of events in the hadronic domain:

$$\begin{array}{cccc} NC(e^-) & NC(e^+) & CC(e^-) & CC(e^+) \\ 5 \times 10^5 & 5 \times 10^5 & 1 \times 10^4 & 5 \times 10^3 \end{array} \tag{21}$$

For NC events the safe region can be enlarged by combining the information from the lepton and the hadronic flow. In particular one has access to the low x regime. Assuming the LL QCD evolution to be valid down to $x = 5 \times 10^{-5}$ one can expect over five millions NC events in the additional range $5 \times 10^{-5} < x < 0.01$ and $0.1 < y$.

The strongest constraint in defining the safe domains, eq. (20), arises from the lower limit in y. In fact, it results in a gap between the kinematical range accessible at HERA and the one presenly explored by fixed target experiments, see Figure 3. For a given value of x the smallest measurable Q^2 at HERA is about 10 times the highest Q^2 reached in H2 target experiments at CERN. This gap can be bridged in part by running HERA at lower energies.

4 Quark momentum distributions

Deep-inelastic lepton-nucleon scattering is the most direct way of exploring the substructure of hadronic matter. At HERA, distances as small as 10^{-3} fm can be probed, indirectly even down to $\sim 5 \times 10^{-5}$ fm. Structure function measurements, thus far restricted to ranges $x \geq 0.03$ and $Q^2 \leq O(100)\,\mathrm{GeV}^2$, can be extended both down to the low-x region and up to high Q^2 values. For example, $O(10^3)$ CC events can be expected with $Q^2 \geq M_W^2$, and more than one million NC events in the interval $10^{-4} \leq x \leq 10^{-3}$ (for $Q^2 \geq 5\,\mathrm{GeV}^2$ and $y \geq 0.01$). A fundamental theoretical test is to check that the measured structure functions are consistent with the prediction of QCD evolution of structure functions measured at lower Q^2. Theoretically very challenging is the low x domain which will become accessible. Here $\ln(1/x)$ contributions are expected [19] to modify the standard QCD evolution based on the LL Altarelli-Parisi formalism. One should also note that a precisce determination of the parton densities (in particular of the gluon at small x) has profound implications for physics at the next generation of very high energy proton proton colliders. Furthermore, structure function measurements can reveal a possible substructure of quarks and leptons.

Two aspects of structure function analysis can be distinguished: (i) the determination of the shape of structure functions and quark momentum distributions in the Bjorken-variable x, and (ii) a detailed analysis of their Q^2 dependence. For the QCD tests (section 6) cross sections differential in x and Q^2 are required. In the former case one can average the resulting x distributions over suitable ranges in y or Q^2 in order to exploit the available statistics. At fixed c.m. energy there are essentially two different procedures [15,20,21] to determine the x shape, an approximative method and one based on exact unfolding of distributions. In the first method one considers a single cross section (or a cross section combiantion) and restricts the kinematical region such that certain structure functions or quark distributions dominate.

The highest statistical precision is achieved for structure functions that can be extracted from just a single NC cross section. The pure electromagnetic structure function, F_2^{em}, can be approximated this way, either by the NC electron or positron cross section. For sufficiently small values of Q^2, Z-exchange can be neglected relative to γ-exchange in eq. (12) and consequently

xF_3 vanishes, while F_2 approaches the electromagnetic structure function F_2^{em} as can be seen from eqs. (13), (14) and (19). In [21] it was shown that, for $x \leq 0.7$ and $y \leq 0.3$, the approximation with a positron beam

$$F_2^{em} = \sum_f e_f^2 (xq_f + x\bar{q}_f) \approx \tilde{\sigma}_{NC}(e^+) \tag{22}$$

is accurate to better than 5% . Similarly as NC cross sections single CC cross sections can be used to approximate quark distributions in restricted kinematical regions. The smaller statistics compared to the NC cross sections is partly compensated by the fact that the W propagator enters the CC cross sections as an overall factor, see eq. (16). Feasible limits are $y \to 0$ and $x \to 1$. For example, at sufficiently large x one can neglect the sea quarks and make use of the valence quark approximations like in

$$xu_v \approx \tilde{\sigma}_{CC}(e^-) \tag{23}$$

Sums and differences of NC and CC cross-sections for e^-p and e^+p scattering allow further separations of individual quark densities.

A more complete separation and determination of structure functions requires the use of all four NC and CC cross-sections measurable in $e^\pm p$ scattering [15,21,22]. At least formally, one can solve the four equations (12) and (16) for four particular quark distributions. A convenient basis is provided by the valence quark densities $u_v = u - \bar{u}$ and $d_v = d - \bar{d}$, and the structure functions $U = u + \bar{u} + c + \bar{c}$ and $D = d + \bar{d} + s + \bar{s}$. The solution is of the form

$$\begin{pmatrix} u_v \\ d_v \\ U \\ D \end{pmatrix} = (A_{ij}) \begin{pmatrix} \tilde{\sigma}_{NC}(e^-) \\ \tilde{\sigma}_{CC}(e^-) \\ \tilde{\sigma}_{NC}(e^+) \\ \tilde{\sigma}_{CC}(e^+) \end{pmatrix} \tag{24}$$

Explicit expressions for the coefficients A_{ij} are given in [21]. The practicability of this method depends on the properties of the transformation matrix A, in particular on its singular behaviour. Since A is a function of x and y containing terms like $[(1-y)^2 A_u(Q^2) - A_d(Q^2)]$ in the denominator there will be certain regions where the unfolding procedure is not applicable. This means that certain distributions can only by unfolded with limited statistics. The necessity to combine (up to) four different cross-sections makes this procedure also subject to larger statistical uncertainties and relative normalization errors compared to the approximate method. Depending on the kinematical region and the considered distribution one or the other method is favourable.

Analyses of structure measurements at HERA have been performed in [15,20,21,22]. They are based on sets of NC and CC Monte Carlo events that correspond to collisions of 30 GeV electrons and positrons with 820 GeV protons for an integrated luminosity of 100-200 pb^{-1} per lepton beam. Systematic uncertainties are only considered through cuts on the kinematical variables as specified in the safe regions eqs. (20). The results are:

- The valence up-quark density can be obtained at $x \gtrsim 0.25$, i.e. in the valence quark region, directly from the CC e^-p cross-section (Fig. 4a), while for smaller values of x the more demanding unfolding procedure based on eq. (24) has to be used (Fig. 4b). The statistical accuracy of the latter is somewhat worse than the accuracy of the approximate, but direct extraction (in spite of the twice as long running time needed for the exact unfolding). Note

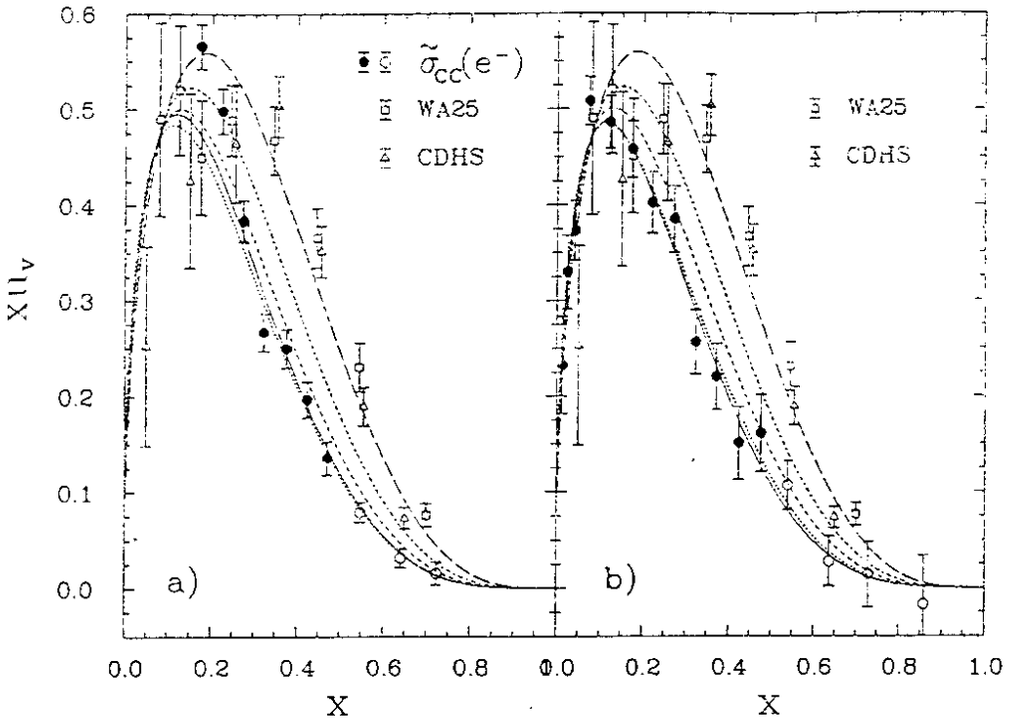

Figure 4: *The valence up-quark distribution $xu_v(x)$: (a) Approximate determination from the CC e^-p cross-section, eq. (23), averaged over $0.03 \leq y \leq 0.3$; (b) Extraction from the NC and CC $e^{\mp}p$ cross-sections, eq. (24), averaged over $0.15 \leq y \leq 1$. The Monte Carlo results correspond to an integrated luminosity of 200 pb^{-1} for e^-p and equally for e^+p collisions, and are drawn as full circles in case the phase space restrictions eq. (20) are satisfied. The curves represent $xu_v(x, Q^2)$ evaluated from the input distributions [23] for $Q^2 = 10$ (long-dashed), 10^2 (dash-dotted), 10^3 (dashed), 10^4 (dotted) GeV^2 and $\overline{Q^2} = x\bar{y}s$ (full), $\bar{y}$ being the average average value of y associated with the MC data. Also plotted are existing measurements of xu_v in neutrino scattering at $Q^2 = 11$ GeV^2 [24] (open squares) and $Q^2 = 15$ GeV^2 [25] (open triangles) with statistical and systematic errors added in quadrature.*

that both methods yield u_v at high values of Q^2, typically around 10^4 GeV^2, i.e. two to three orders of magnitude above presently accessible scales. As illustrated in Fig. 4, it should be possible to check the evolution of xu_v predicted by QCD at least in a rough way.

- A separate determination of the valence down quark density is difficult. However, useful constraints can be derived in the valence quark regions and from the sum and differences of the valence up and down quark distributions, $x(u_v \pm d_v)$, which can be extracted in various ways.

- The total flavour singlet structure function, $F_s = \sum_f x(q_f + \bar{q}_f)$, can be measured rather good at average values of Q^2. The best possibility is provided by a combination of the CC cross sections for e^+p and e^-p scattering.

- It is also possible to separate the charge 2/3 from the charge 1/3 quark distributions, xU and xD, respectively, using the exact unfolding relations (24). On the other hand, a

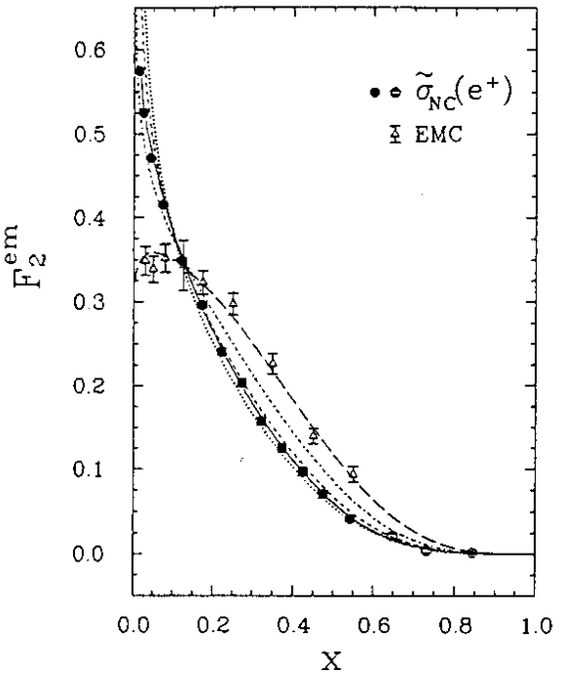

Figure 5: *Determination of the electromagnetic structure function F_2^{em} from the NC e^+p cross-section, eq. (22), averaged over $0.03 \leq y \leq 0.3$. Further explanations on the MC result and the curves are given in Fig. 4. Also plotted is an existing measurement of F_2^{em} in muon scattering at $Q^2 = 11.5$ GeV^2 [26] (open triangles) with statistical and systematic errors added in quadrature.*

separation of sea quarks from valence quarks is more difficult. Such a separation appears possible only at large y. Nevertheless, the charge 2/3 quark sea distribution xU_{sea} and the total quark sea distribution xS ($S \equiv \sum_f (q_f + \bar{q}_f) - u_v - d_v$) can be obtained with satisfactory statistical accuracy. However, no way was found for a meaningful determination of the charge 1/3 quark sea distribution xD_{sea}.

- Finally, F_2^{em} is the structure function that can be determined most accurately. The statistical errors for a run of 200 pb^{-1} are, in fact, so small that the corresponding error bars lie inside the MC data symbols drawn in Fig. 5. Moreover, the departure of F_2^{em} from the actually measured distribution $\tilde{\sigma}_{NC}(e^+)$ is smaller than the statistical errors as long as $Q^2 \lesssim 3000$ GeV^2 or $y \lesssim 0.3$. This can be seen from the precise agreement between the theoretical expectation on $F_2^{em}(x, \overline{Q^2})$ represented by the full curve in Fig. 5 and the MC data on $\tilde{\sigma}_{NC}(e^+)$. The clear change in shape of the MC result as compared to the existing EMC data on F_2^{em} at $Q^2 \simeq 10$ GeV^2 shows rather impressively the observability of the QCD evolution. Thus F_2^{em} will play the most important role for more quantitative QCD tests [15,16]. In addition, F_2^{em} can also be measured very well in the region $10^{-4} \leq x \leq 10^{-2}$ as discussed in [15,20], and thus may serve as a sensitive probe of low-x physics.

5 Gluon momentum distribution

An important conclusion from all attempts to derive parton distributions from current data is that the gluon distribution is very poorly determined at small x ($< O(10^{-1})$) [27]. Apart from the intrinsic interest of a measurement of the gluon distribution at small x, such a measurement will also have important consequences for other physics topics at HERA. For example, the prospects to determine Λ_{QCD} at HERA can be substantially improved by a better knowledge of the gluon below $x < 0.01$ [15]. We note in passing that the size of the gluon distribution at small x is of great importance for physics at the next generation of very high energy proton proton colliders. For example, cross sections for $b\bar{b}$ production depend sensitively on the gluon at small x. Several methods have been proposed by which HERA can provide information on this important question.

An accurate measurement of the longitudinal structure function, $F_L(x, Q^2)$, in the small x region can lead to an accurate determination of the gluon distribution in the same x region. The key theoretical input is the fact that at small x the dominant contribution to F_L comes from the gluon distribution, see eq. (18). At HERA one will be able to reach very small x values and still have large enough Q^2 values that QCD calculations at leading twist are applicable. In [28] a full analysis of the experimental systematic errors and the measurement requirements has been performed. It was shown that the final state electron can be clearly identified and well measured for events at small x ($10^{-3} \leq x \leq 0.05$) and moderate Q^2 ($25 < Q^2 < 150\,\mathrm{GeV}^2$) over a broad range of proton beam energies. Provided that HERA is run at a reduced c.m. energy, for example with a proton beam energy of 500 GeV, for an integrated luminosity $\geq 30\,\mathrm{pb}^{-1}$, one will be able to obtain measurements of $F_L(x, Q^2)$ which are accurate enough to extract the gluon distribution at small x, and hence to distinguish between the widely differing forms which are currently proposed, all of which are consistent with present data.

An entirely different way of obtaining information on the small x gluon distribution is provided by inelastic J/Ψ production at low Q^2, Figure 1a. Here one makes use of the theoretical result

$$\frac{d\sigma}{dx}(\gamma p \to J/\Psi\, X) = xG(x, M_\Psi^2)\, \frac{\Gamma_{ee}}{M_\Psi^3}\, f\left(x, \frac{s_{\gamma p}}{M_\Psi^2}\right) \tag{25}$$

with f a known function which is sharply peaked at small values of x. Eq. (25) is expected to be valid for $z = pp_\Psi/pq \leq 0.8$ and $p_\perp^2 \geq 0.1 M_\Psi^2$. It follows that the inelastic photoproduction cross section, $\gamma p \to J/\Psi\, X$, integrated over x is, to a very good approximation, proportional to the gluon distribution at a particular value of x of order $M_\Psi^2/s_{\gamma p}$. The forward electron spectrometer in the ZEUS experiment permits measurements of $Q^2 \approx 0$ photons in the range eq. (6) which means that x values of order of 10^{-3} can be probed. The cross section $\sigma(ep \to J/\Psi\, X; J/\Psi \to l^+l^-)$ is $O(10\,\mathrm{pb})$. A full detector simulation and error analysis has been performed in [29]. It was found that a good discrimination between different sets of gluon distributions should be achievable.

Bottom quark production provides another mechanism for J/Ψ production via the decay $b \to J/\Psi\, X$. The $b\bar{b}$ production process $\gamma p \to b\bar{b} \to b\, X$ has a harder $p_\perp$ distribution and is more shifted towards small values of z. Thus it seems feasible to distinguish the two mechanisms for producing J/Ψ's [30,31]. Useful are cuts on the kimenatical variables $p_\perp$ and z, and signatures exploiting the different event topology. J/Ψ's are within a jet for $b\bar{b}$ events and more isolated in inelastic production.

Both methods presented so far require a rather long running time: the J/Ψ cross section is rather small, and the method based on the measurements of F_L requires two runs at different cms energies. In contrast, the NC boson-gluon cross sections, $\gamma/Z + g \to q + \bar{q}$, are large, of the order of several μb. The problem here is how to tag these events. One can use for instance heavy quark events. In [5] it was shown that photon-gluon fusion is the dominant source of charm and bottom production at HERA. One expects $O(10^8)$ charm and $O(10^6)$ bottom events per year. These events are photoproduced and for a fair fraction the scattered electron might be seen in the forward electron/photon detector. Obvious tags of heavy flavour events are large $p_\perp$ leptons from their semileptonic decays. For example, requiring an isolated lepton with $p_\perp \geq 3.5\,\mathrm{GeV}$ $O(10^4)$ tagged bottom events are estimated. Since heavy quarks are mainly produced closed to threshold, the x of the gluon can be approximated by $x_g = (Q^2 + \hat{s})/(ys) \approx 4m_Q^2/(ys)$. Thus the gluon density will be mainly probed in the low x ($x < 0.01$) region at a scale of the order of the heavy quark mass. The main problem is the determination of the invariant mass, $\hat{s}$, of the heavy quark subsystem.

Light quark events can also be used to extract the gluon distribution, both in photoproduction and in DIS. The signature of photoproduced $\gamma p \to q\bar{q}X$ events are two recoiling jets at high $p_\perp$. The gluon will then be probed at $x_g = O(p_\perp^2/s)$ and with a scale of order $p_\perp$. Serious backgrounds will not only come from the pointlike QCD compton process, $\gamma q \to qg$, but also from the anomalous photon contributions. Signatures based on differences in the distributions of jet-$p_\perp$, rapidity, and the angular of the dijet system as a function of the dijet mass have to be exploited to identify the gluon initiated process. For DIS events the background from resolved photon contributions is absent. Here the mass scale governing the gluon density is Q^2 which can be measured with help of the scattered lepton. Problems are the x of the gluon which is not directly accessible, $x_g = x(1 + \hat{s}/Q^2)$, and the background processes $\gamma q \to q$, $\gamma q \to qg$ as well as higher order processes. An attempt to measure the gluon density from DIS photon-gluon events has been made in [32] using a numerical unfolding procedure applied to a Monte Carlo data sample enriched in these events using topological criteria. In particular, correlations between the gluon momentum fraction x_g and observable quantities were established. Again a distinction between different gluon density parametrization seems feasible.

A constraint on the gluon momentum distribution can also be obtained from a QCD analysis of the Q^2 evolution of structure functions. The analysis of F_2^{em} in [15] shows that the fitted value of Λ_{QCD} depends crucially on the choice of the parametrization for the input gluon density, $xG(x, Q_0^2)$. The prospects to obtain a useful result on $xG(x)$ depend on the minimum x value. Considering HERA data with $x > 0.01$, where the normal LL QCD formalism is expected ot be valid, a simultaneous measurement of the gluon distribution and Λ from the Q^2 variation of F_2^{em} cannot be made with errors small enough to be of interest, even if HERA is run at lower energy. At x below 0.01 events are abundant and well measurable at HERA. Higher order QCD effects, involving $\ln(1/x)$ terms, are expected to be relevant in this region [19]. A calculation performed in [33] seems to indicate that the effect of these contributions on the gluon density is less than 15% even if $x \sim 10^{-4}$. By extending the LL analysis down to $x = 10^{-3}$ a reliable determination of xG seems feasible [15]. It was found that the error contours at low x are sufficiently separated to allow a discrimination between different parametrizations of the gluon.

6 QCD analyses

Present measurements of the logarithmic scaling violation of DIS structure functions as predicted by (massless) QCD in fixed target experiments are strongly limited by power-behaved

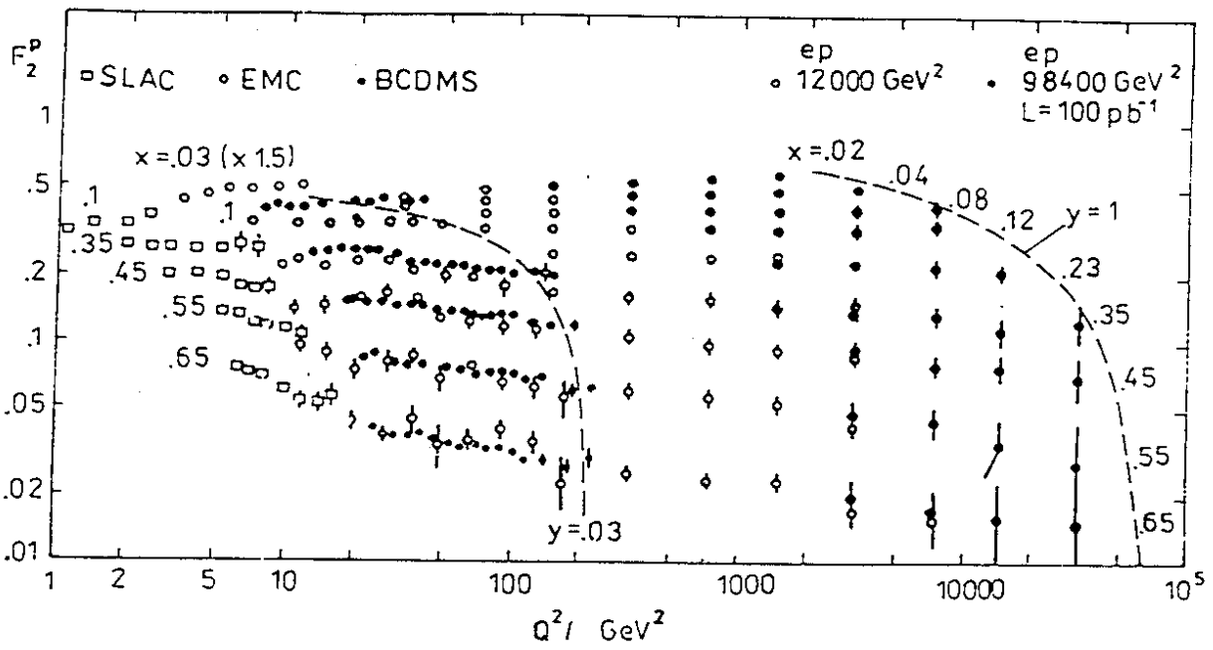

Figure 6: *$F_2^{em}(x, Q^2)$ for $1 < Q^2 < 10^5$ GeV^2 as measured by different fixed target experiments compared with HERA. The dashed curves are for $y = 1$ at $\sqrt{s} = 314$ GeV and for $y = 0.03$ at $\sqrt{s} = 110$ GeV. Note that even at the lowest cms energy $\sqrt{s} = 110$ GeV HERA data will have no overlap with SPS measurements. The Monte Carlo results for HERA correspond to an integrated luminosity of 100 pb^{-1} for e^-p collisions. From [15].*

corrections in Q^2 like finite mass effects and higher twist operators. Due to the higher Q^2 at ep colliders the $\ln(Q^2)$ QCD effects will clearly dominate over the non asymptotic background. Also, a larger lever arm in Q^2 can be expected. In contrast to this there are new complications like a reduced sensitivity to Λ at high Q^2, power behaved Q^2/M_Z^2 effects from the Z propagator, additional structure functions entering the differential cross section formula, and the restricted accessible kinematical range. Examinations of the possibilities and requirements of testing QCD through scaling violation in structure function at HERA have been performed in [15,16].

In Figure 6 [15] two measurements of F_2 as expected at HERA at $\sqrt{s} = 314$ GeV and $\sqrt{s} = 110$ GeV are superimposed on charged lepton-proton scattering data from SLAC and the CERN SPS muon experiments [26,34,35], suppressing a few data points at low x. Though the combined measurements extend over almost five orders of magnitude in Q^2 there remains a gap between HERA and present day data even when running HERA at lower energy arising from the severe constraint on y. For a given value of x the available Q^2 range is substantially reduced, in particular at high $\sqrt{s}$. It is clear that enlarging the accessible kinematical range and/or lowering the cms energy would improve a Q^2 analysis.

As emphasized in [15,21] F_2^{em} is the structure function best suited for QCD tests. It is not only the one that can be measured with the highest statistical precision at HERA but depends moreover only on two input distributions besides the gluon distribution. Furthermore, the weight factors of its decomposition into a singlet and non-singlet component are simple numbers:

$$F_2^{em}(x, Q^2) = \frac{1}{6}\Delta_p(x, Q^2) + \frac{5}{18}F_S(x, Q^2) \tag{26}$$

Data			$g(x,Q^2)$	$\Delta_{stat}\Lambda$
cms energy	y_{min}	x_{min}		[MeV]
high s	0.03	0.01	fitted	135
high s	0.03	0.01	fixed	25
high s	0.03	0.25	non-singlet	176
high s	0.01	0.01	fitted	76
low s	0.03	0.01	fitted	58
high s	0.03	10^{-4}	fitted	25

Table 1: *Statistical error on Λ_{QCD} from QCD fits of F_2^{em} from data at the nomimal HERA energy ("high s") of $\sqrt{s} = 314\,GeV$ and from data at lower energy of $\sqrt{s} = 134\,GeV$. The integrated luminosity is $200\,pb^{-1}$ for $\sqrt{s} = 314\,GeV$ and $100\,pb^{-1}$ for $\sqrt{s} = 134\,GeV$. From [15,16].*

Here Δ_p is the non-singlet distribution $\Delta_p = \sum_i (u_i + \bar{u}_i - d_i - \bar{d}_i)$ and $F_S = \sum_i [q_i + \bar{q}_i]$. In contrast, the full NC cross section, eq. (12), which could be analyzed in the full kinematic range is a superposition of a singlet and three non-singlet functions (besides xG) and the Altarelli-Parisi equations have to be modified to take the (y, Q^2) dependence of the weight factors into account. An analysis of the Q^2 evolution of F_2^{em} in the LL approxiamtion has been performed in [15,16] based on the Laguerre technique developed in [36]. This method has the advantage that the input distributions $\Delta_p(x, Q_0^2)$, $F_S(x, Q_0^2)$ and $G(x, Q_0^2)$ can be extracted from the data without any prejudices concerning their particular analytic form. Furthermore the necessary multiparameter fit can be reduced to solving a system of linear equations and to one parameter minimization for Λ. The Monte Carlo data sample were generated using the parton density parametrization of [37]. The result of the statistical precision for Λ corresponding to an integrated luminosity of $200\,\mathrm{pb}^{-1}$ is given in Table 1 [15,16]. Systematic uncertainties are only considered through cuts on the kinematical variables. A first analysis of the systematical uncertainties in [16] indicates that the systematic error on Λ approximately equals the respective statistical error on Λ given in Table 1. The main points of the statistical analyses are:

- The determination of Λ from the high energy data alone with $x > 0.01$ yields $\Delta\Lambda$ of about 135 MeV. The main limitation is the unknown gluon density.
- As discussed in section 5 there may exist different possibilities to measure xG at HERA. If the gluon distribution would be known exactly the statistical error were reduced to about 25 MeV.
- Another way to avoid the gluon density is a non-singlet analysis in the valenece quark region. Since this restricts $x > 0.25$ the uncertainty in Λ does not improve for $y > 0.03$, $\Delta\Lambda \approx 176\,\mathrm{MeV}$.
- The lever arm in Q^2 is strongly limited by the lower cut in $y > 0.03$. A possible extension

Contact: Λ_{eq}	4-7 TeV[47]
excited e^*	200 GeV[44]
leptoquarks	300 GeV[42]
leptogluons	280 GeV[42]
$\tilde{e}+\tilde{q}$	180 GeV[45]
Z'	200-300 GeV[41]
$W_R^{\pm}$	300-400 GeV[41]
$Z_R^{\pm}$	350-470 GeV[41]
top quark	70-80 GeV[49]
$WW\gamma$: $\Delta\kappa$	0.5[40]

Table 2: *Estimated limits on new particles and interactions at HERA.*

of the safe region to $y > 0.01$ improves the statistical precision in general. For example, from 135 MeV to about 76 MeV at $x > 0.01$.

- A larger range in Q^2 can also be obtained by running HERA at lower cms energy. Data at low $\sqrt{s} = 134$ GeV give $\Delta\Lambda = 58$ MeV at $x > 0.01$ and $y > 0.03$.

- Due to the dominant role of the gluon distribution at low x the error of Λ depends strongly on the lower limit x_{min}. Extending the LL analysis to $x < 0.01$ one obtains impressive small statistical errors, 25 MeV for $x_{min} = 10^{-4}$ at $y > 0.03$ and $\sqrt{s} = 314$ GeV. This underlines the importance of studies of the low x domain at HERA.

7 New physics possibilities

HERA, like any other accelerator exploring a new energy domain, has certain opportunity windows for discovering "new physics". Given the cms energy of $\sqrt{314}$ GeV and momentum transfers up to $Q^2 \sim 4 \times 10^4\,\mathrm{GeV}^2$, it will be possible to produce new particles with masses up to 300 GeV and to test for new interactions down to distances $r_{min} \sim (200\,\mathrm{GeV})^{-1} \sim 10^{-16}$ cm. The highest masses of new (and known) particles are accessible in single particle resonance production. The list of particles includes leptoquarks, leptogluons, excited quarks and leptons, the W and Z bosons, and a heavy top quark ($m_t \geq 55$ GeV). If the particles carry a conserved quantum number they can only be produced in pairs. An example is the production of supersymmetric particles. Exploiting indirect signals one can of course set limits on new physics far above the HERA cms energy. These indirect effects of physics beyond the SM, well below its own threshold, show up as deviations of suitable quantities from their SM values. Prospects at HERA are the measurement of a possible anomalous magnetic moment of the W, anomalous effects in B^o-$\bar{B}^o$ mixing, new weak currents and last not least a new level of substructure below that of quarks and leptons. A summary of the physics reach of HERA is

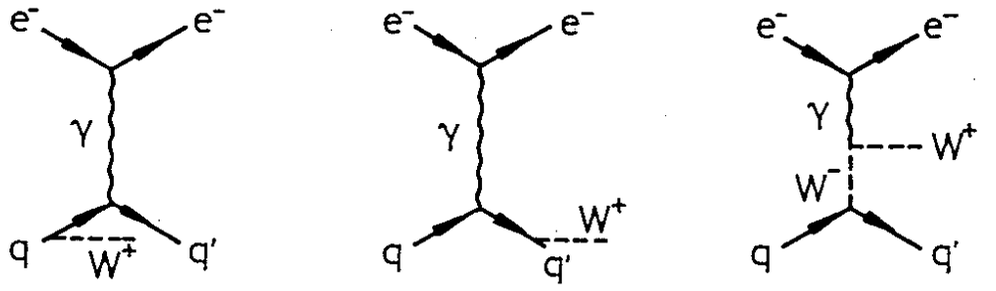

Figure 7: *Dominant graphs in W^+ production at HERA.*

given in Table 2. The individual items will be discussed in more detail in the following.

The computational work on the production of bosons with ep colliders is extensive, see [38] for references. The weak W and Z bosons can be produced by bremsstrahlung from a lepton or quark line and by boson fusion, γW, WW, WZ, exhibiting a triple gauge boson vertex. The NC photon exchange diagrams give the largest contribution. Thus the dominant subsets are given by the photon exchange diagrams with emission from the quark lines and the γW fusion diagrams (to preserve gauge invariance), see Figure 7. Since the total cross section is dominated by small Q^2, pointlike and resolved photon contributions have to be considered with an appropriate caveat of double counting. Including the small contribution from quasi-elastic scattering the following numbers of weak bosons can be expected at $100\,\mathrm{pb}^{-1}$ [38]: 53 W^- events, 40 W^+ events, and 25 Z° events.

As was pointed out in [39] a large cancellation occurs between the non-Abelian contributions and the leptonic (or hadronic depending on the process under consideration) contributions, compare Figure 7. Thus a small deviation of the triple gauge boson coupling in the SM will suppress or remove this compensating effect. Measurements of the triple gauge boson couplings could not be performed so far. Both the e^+e^- machines LEP 1 and SLC and the hadron collider Tevatron can only place weak limits on the parameter κ and λ quantifying the deviation of the gauge boson couplings from their SM values $\kappa = 1, \lambda = 0$. At the Tevatron a bound not better than $-3 \leq \kappa \leq 5$ is expected. In W pair production at LEP2 it is a combination of $WW\gamma$ and WWZ couplings which is measured. Thus the independent measurements of $WW\gamma$ couplings is a challenge for HERA, feasible several years before LEP will reach sufficiently high energies to produce W pairs. A first study on the sensitivity of W production at HERA to a possible anomalous magnetic moment of the W was performed in [40] using as signature inclusive W event rates within certain cuts. The signal of W events consists of a high transverse momentum ($p_\perp$) electron or muon plus large missing transverse momentum ($\not{p}_\perp$) due to the associated neutrino in W leptonic decay, a jet produced by the quark struck inside the proton and, possibly, the original beam electron. Hence the cuts are based on a jet $+l+\not{p}_\perp$ signal. If the normalization of the SM rate within cuts is known within $\sim$ 15% then, at $200\,\mathrm{pb}^{-1}$ and to $1\,\sigma$, the following limits on κ and λ can be reached at HERA: $-1.8 \leq \lambda \leq +1.8$, and $-0.5 \leq \kappa - 1 \leq +0.4$. The limits on κ look indeed promising.

The prospects for SM Higgs-boson physics at HERA are poor [38]. The WW fusion diagram yields the main contribution to the Higgs boson, H°, production. Over a wide range of the Higgs boson mass the CC production is about a factor seven larger than the NC production. For the latter the contribution from $\gamma\gamma$ fusion amounts only to about 10% of the ZZ fusion contribution. The total cross section for producing a Higgs boson at HERA is of the order of

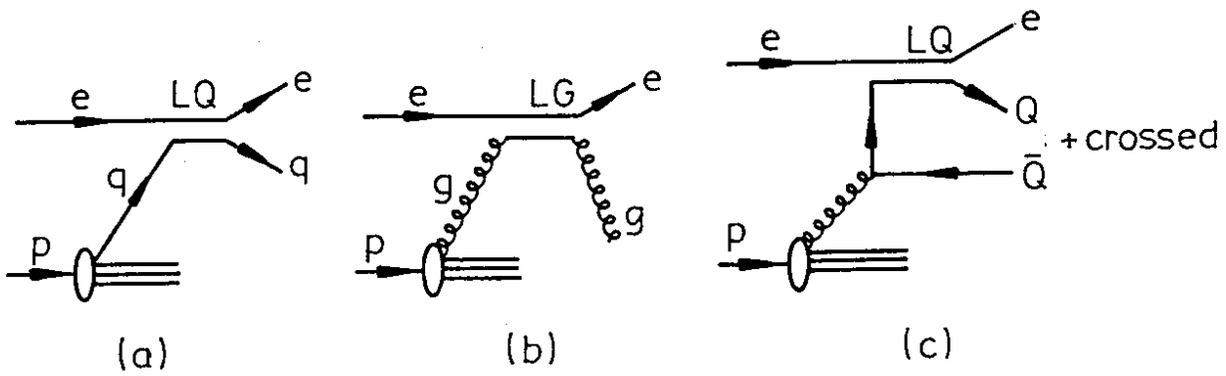

Figure 8: *Direct channel production of leptoquarks LQ (a) and leptogluons LG (b), and associated production of heavy leptoquarks (c) in ep scattering.*

0.02 pb for $M_H = 20$ GeV weakly decreasing with increasing M_H. Though some events can be expected they can hardly be distinguished from the large background of heavy quarks since the Higgs boson will dominatly decay into $b\bar{b}$ or, if possisble into a $t\bar{t}$ pair. Even $\bar{t}b$ production with $m_t = 80$ GeV is about a factor five larger than the dominant CC signal process $e^- p \to \nu_e H^o X$. The production rates for non-standard Higgs bosons are somewhat larger but nevertheless too small to be exploited in the direct channels at HERA.

The prospects of detecting new weak gauge bosons at HERA has been investigated in [41]. Given the low production rates for the ordinary W and Z bosons it seems impossible to observe the direct production of W' and Z' in some suitable decay channels. Indirect searches will make use of the fact that the inclusive NC and CC cross sections for $e^{\mp}_{L,R} p$ scattering will be modified. Firstly, there are deviations of the interactions involving the lighter (standard) bosons from the SM due to Z-Z' and W-W' mixing, and secondly there are additional contributions from the exchange of the heavier bosons. In [41] it was found that the sensitivity to new weak gauge bosons depends rather strongly on their properties, i.e. on the particular model considered. With unpolarized cross sections one can reach Z' masses of about 350 GeV and masses of about 300 GeV for an extra W' coupling to right-handed currents. This range can be extended by 10% to 40% with the help of polarized beams. Polarization experiments are particularly convenient in determining Z' and W' couplings and distinguishing models. On the other hand it will be difficult to improve the existing constraints on Z-Z' and W-W' mixing angles at HERA.

HERA can contribute the strongest experimental information on new physics if the exotic excitations are preferentially connected with the quark-lepton (or gluon-lepton) channel. Leptoquarks, objects with the quantum numbers of both leptons and quarks, and leptogluons are ideal exotic candidates for HERA. Leptoquarks (LQ) arise in a number of theoretical scenarios (composite models, GUT theories, superstring inspired models), while leptogluons (LG) are more speculative [42]. LQ's and LG's correspond to direct channel resonances, Figure 8a and b. For masses below the production threshold the large production rates together with a clean signature, a δ-function like peak in the x distribution at $x = m^2/s$, allow a detection up to close the HERA kinematical limit [42]. A detection above the HERA threshold seems to be difficult since the interference of the LQ with the NC contributions below the LQ peak is rather small. At HERA also a different sort of leptoquarks can be produced which couple proportional to the mass of the relevant quarks and leptons. The Feynman diagrams of their associated production

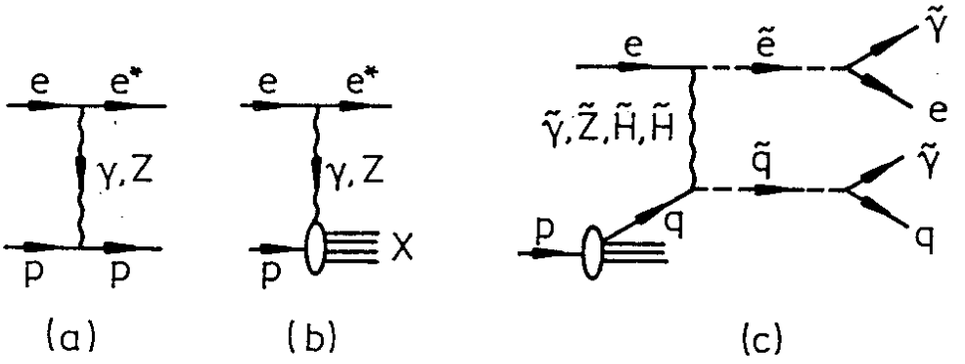

Figure 9: *Feynman diagrams for excited electron production in elastic (a) and inelastic (b) ep collisions. (c) Squark and selectron production in ep scattering.*

with a heavy quark (top or bottom) in electron-gluon scattering are shown in Figure 8c. A signal up to a mass of about 100 GeV seems feasible [42].

Excited leptons (l^*) and quarks (q^*) are a generic prediction of composite models. Their search is a classical field of interest in ep scattering. q^* and e^* production cross sections are smaller than LQ cross sections because they require a Bremsstrahlung photon. The cross section for elastic e^* production ($ep \to e^*p$, Figure 9a) turns out to be of the same order of magnitude as that for inelastic e^* production, Figure 9b [43]. The elastic channel has a very clean signature: nothing but a wide angle electron-photon pair from the decay of the e^* in the detector. The limiting background comes from wide angle bremsstrahlung, $e + p \to e + p + \gamma$. The conclusion of the analysis in [44] is that an excited electron e^* up to a mass of $\sim$ 200 GeV can be discovered at HERA.

The scalar partners of electrons and quarks, selectrons $\tilde{e}$ and squarks $\tilde{q}$, predicted by supersymmetry, can only be produced in pairs. Among all possible supersymmetric production processes at HERA the most promising one is the process $ep \to \tilde{e}\tilde{q}X$, shown in Figure 9c [45]. The signature is very nice. The produced spartners decay into electrons and quarks plus photinos (which produce missing energy), giving rise to events which are unbalanced in the transverse plane. Given the present limits on the mass of squarks and selectrons, HERA still has a narrow window open for the detection of supersymmetric signals, 100-120 GeV $\leq m_{\tilde{e}} + m_{\tilde{q}} \leq$ 160-180 GeV.

The search for a substructure of quarks and leptons was one of the motivations for building the ep collider HERA. If quarks and leptons are composite at a scale $\Lambda \gtrsim O(1\,\mathrm{TeV})$ then, clearly, at energies $E \gtrsim \Lambda$ their composite nature should become manifest. Yet, one can also expect observable effects at energies $E < \Lambda$. An essentially unavoidable consequence of compositeness are residual interactions induced by the strong binding force. These contact interactions interfere with the conventional gauge interaction and yield deviations of order $Q^2/(\alpha\Lambda^2)$ from the SM expectations [46]. Since $\alpha \ll 1$ these effects are already observable at $Q^2 \ll \Lambda^2$. In ep collisions, one can test lepton-quark contact interactions and bound the scale parameter Λ_{eq}. It should be noted that other phenomena beyond the SM, occuring at a large scale Λ, will give rise to effective interactions similar to those considered in the case of substructure. An example are virtual effects of new particles.

Low energy effects of new physics, characterized by a mass scale $\Lambda > 1/\sqrt{G_F}$, can be systematically studied by means of an effective, nonrenormalizable lagrangian L_{eff}. The most important operators are four-fermion operators which have dimension 6 and, therefore, dimensionful coupling constants g^2/Λ^2 yielding the following (helicity conserving) lagrangian [46]

$$L_{eff} = \frac{g^2}{\Lambda^2}\{\eta_{LL}(\bar{e}_L\gamma_\mu e_L)(\bar{q}_L\gamma^\mu q_L) + \eta_{RR}(\bar{e}_R\gamma_\mu e_R)(\bar{q}_R\gamma^\mu q_R) + \eta_{LR}(\bar{e}_L\gamma_\mu e_L)(\bar{q}_R\gamma^\mu q_R) + \eta_{RL}(\bar{e}_R\gamma_\mu e_R)(\bar{q}_L\gamma^\mu q_L)\} \quad (27)$$

The coefficients η_{ab} take the values ± 1 and 0, and one may plausibly take $g^2/(4\pi) = 1$ leaving Λ as a free parameter. The scattering amplitudes obtained from this lagrangian interfere with the SM amplitude from γ- and Z-exchange and will be observable in the Q^2 distributions of the differential cross sections $d\sigma(e^\pm p \to e^\pm X)/dQ^2$ and in various asymmetries $A(Q^2)$. A quantitative analysis shows that the effects of the contact interactions eq. (27) will be observabie at HERA for values of Λ up to 4-7 TeV for an integrated luminosity of $100\,\mathrm{pb}^{-1}$ [47]. Thus HERA will allow insight in the structure of matter down to distances of the order of 10^{-5} fm in this scenario! Moreover, it turns out that polarized beams will greatly help to disentangle the helicity structure of contact interactions in case of a positive signal.

Interactions invariant under $SU(3)\times SU(2)\times U(1)$ symmetry may also change the helicity at the quark and lepton vertex. In [48] it was demonstrated that a pure tensor contact interaction is the only interaction consistent with the constraints from rare decays. Contrary to all current-current interactions it generally leads to a violation of the Callan-Gross relation in ep scattering. In fact, the chirality changing tensor contact interaction gives a positive contribution to $R = (2xF_1 - F_2)/(2xF_1)$ which is approximately independent of x. In contrast, scalar partons inside the proton would contribute only to F_2 and not ot F_1 and hence give a negative contribution to R. Similarly, QCD corrections yield significant deviations from $R = 0$ only at small values of x. Hence, a precise determination of structure functions at HERA will provide bounds on chirality changing contact interactions. If R will be measured with 10% accuracy, a bound on Λ of about 2 TeV appears feasible.

Searching for the top quark is a major challenge at every new accelerator giving access to higher energies in different kinds of interactions. Top quark production at HERA is expected to be dominated by the process of boson-gluon fusion, which occurs in first-order QCD [50,11]. In neutral current interactions a $t\bar{t}$ pair is produced, whereas the charged current process gives rise to a $\bar{t}b$ pair. The latter process dominates if the top quark mass is larger than about 55 GeV, due to the lower threshold for single top production as compared to pair production. Given the present top quark mass limits of about 50-60 GeV, the production cross-section is unfortunately small and decreases rapidly with increasing mass. At $200\,\mathrm{pb}^{-1}$ one expects, for instance, about 820 events for $m_t = 40\,\mathrm{GeV}$, ~ 62 events for $m_t = 60\,\mathrm{GeV}$ and ~ 10 events for $m_t = 80\,\mathrm{GeV}$. The statistical limitations with only a few events in the remaining samples, after cuts to reduce the background, will therefore be a severe problem. We note, however, that the numbers given above are probably to pessimistic. Uncertainties in the cross section calculations are discussed in [51]. Varying the mass scale that governs the strong coupling constant α_s and the gluon density can lead to a factor two larger top cross section. The full next-to-leading order corrections, expected to dimish the mass scale uncertainty, have not been calculated so far. An estimate of next-to-leading effects on $t\bar{t}$ production in ep scattering was obtained in [51] based on the inclusive $O(\alpha_s^2)$ calculation of photoproduction of heavy quarks in [52]. According to this approximation, top quark production increases by roughly a factor of two and becomes less sensitive to changes of the mass scale. An estimate of $O(\alpha_s^2)$ effects on $\bar{t}b$ production can not be obtained this way and is still an open question.

Strategies for a top search at HERA have been investigated in [49]. It was found that a clean signal can be obtained up to a mass of $\sim$ 80 GeV exploiting the signature of semileptonic top decays in $\bar{t}b$ events. A proper mass determination seems, however, to be limited to 60-70 GeV. On the one hand, the top mass cannot be reconstructed in semileptonic top decays of $\bar{t}b$ events due to the presence of two high energy neutrinos. On the other hand, the large multijet background of light quark CC events can produce the same signature as the nonleptonic top decays of $\bar{t}b$ events and is furthermore rather uncertain in magnitude since it can (presently) only be treated through leading-logarithm parton cascade methods. In contrast, both semileptonic and nonleptonic decay channels of $t\bar{t}$ events were shown to peak in suitable mass distributions allowing thus a top mass determination up to 60-70 GeV. Yet, there are some perspectives to improve on signatures based on the $\bar{t}b$ sample: use of a positron beam instead of an electron beam, longitudinal lepton polarization, a more reliable description of multijet backgrounds, observation of secondary vertices, possibilities to tag bottom particles, and last not least increased luminosity and/or higher cms energy.

8 Electroweak tests

Though the production rates of real W and Z bosons are non negligible, quantitative tests will be provided by the charged and neutral weak currents and the W and Z propagators. Needless to say that measurements of M_Z at LEP and SLC are expected to yield $\sin^2\theta_W$ to within ± 0.0005 if m_t and M_H were known independently. A precise measurement of just one quantity is not sufficient. The top and Higgs masses will introduce uncertainties of $\approx \pm 0.002$ in the extraction of $\sin^2\theta_W$ from M_Z as long as they have not been measured. In order to test the consistency of the SM at the level of the radiative corrections, to constrain M_H and m_t, to search for new physics, and to obtain the best average value on e.g. $\sin^2\theta_W$, it is necessary to combine several high precision experiments. A number of existing and planned electroweak tests are listed in Table 3. The weak neutral current of lepton-quark scattering has always provided one of the major quantitaive tests of the SM. In fact, deep inelastic neutrino scattering on an isoscalar target, νN, has so far yielded the most precise value on $\sin^2\theta_W$, see Table 3. Comparison of NC data (at low Q^2) with the W and Z masses ($Q^2 \approx M_W^2$) establishes the existence of radiative corrections at the 1σ level. With the ep collider HERA it will become possible to test the weak current over a wide Q^2 range up to $Q^2 \approx 10^4$. In view of the great success of existing (low Q^2) NC experiments it is instructive to compare these fixed target lepton quark scattering experiments with the ep collider HERA. There are essentially three types of lepton-quark scattering experiments: (i) νN, (anti-) neutrino scattering from (approximately) isoscalar targets by CDHS and CHARM (CERN), by CCFERR and FMM (FNAL), and in a number of earlier experiments; (ii) μC deep inelastic scattering by BCDMS; and (iii) electron-quark scattering in the SLAC eD experiment. Two features are common to all these experiments, firstly the high statistics available, cf. Table 3, and secondly the fact that the maximum $Q^2 \ll M_W^2$ such that one is not sensitive to any propagator effects. On the other hand one can safely neglect terms $O(Q^2/M_W^2)$ which simplifies the analyses and the calculation of the radiative corrections. The (anti-) neutrino experiments are the most powerful ones since they proceed via purely weak processes and can thus explore both the NC ($\nu_l \to \nu_l$) and the CC ($\nu_l \to l$) which appear with roughly the same size. Using the (experimentally measurable) antineutrino over neutrino cross section ratio, $r = \sigma^{CC}(\bar{\nu})/\sigma^{CC}(\nu)$, or equivalently QCD evolved structure functions one can extract $\sin^2\theta_W$ from the NC over CC cross section

reaction	experiment	$< Q^2 >$[GeV^2]	# events	exp. quantity	$\sin^2\theta_W$	$\Delta \sin^2\theta_W$	comment
atomic p.v.	Boulder,Paris	10^{-6}		$\mathrm{Im}E_1^{pv}/\beta$	0.209	$\pm 0.018 \pm [0.014]$	$-Q_W(N,Z)$
						± 0.003	1990's
$\nu_\mu e^- \to \nu_\mu e^-$	E734, CHARM	10^{-2}	100	$\sigma^{\nu,e}$	0.223	$\pm 0.018 \pm [0.002]$	no strong int.
	CHARM II (LCD)					± 0.005 (± 0.002)	1989 (1990's)
νN	CDHS,CCFRR etc.	50	500k	$R_\nu = \sigma(NC)/\sigma(CC)$	0.233	$\pm 0.003 \pm [0.005]$	no propagator, $\nu \to l, \nu \to \nu$
μC	BCDMS	100	$\geq 1M$	$B(\lambda = 0.8) = \frac{\sigma^+ - \sigma^-}{\sigma^+ + \sigma^-}$	0.25	± 0.08	no CC statistics, interference
eD	SLAC	100	high	$A(\lambda = .37) = \frac{\sigma_R - \sigma_L}{\sigma_R + \sigma_L}$	0.221	$\pm 0.015 \pm [0.013]$	larger ew corrections
ep	HERA	10–10^4	CC: 10k	$R(\lambda) = \sigma(NC)/\sigma(CC)$		$\pm 0.002 \pm [0.002]$	enough $\sigma(CC)$, propagator (1991)
$p\bar{p} \to W, Z$	UA1,2	10^4	100	M_W, M_Z	0.228	$\pm 0.007 \pm [0.002]$	
	ACOL, Tevatron		10^3			± 0.003	(1990)
e^+e^-	PETRA, TRISTAN	10^3	high	A_{FB}, R	0.232	± 0.011	
	SLC,LEP	10^4	10^4	M_Z, G_μ		± 0.0005	$\Delta M_Z = 45$ MeV
				A_{LR}		± 0.0003	polarization?

Table 1: *Determination of* $\sin^2\theta_W$ *from various reactions, from [41] and [42] (e^+e^-). The central values of all fits assume* $m_t = 45\ GeV$ *and* $M_H = 100\ GeV$ *in the radiative corrections. Where two errors are shown the first is experimental and the second (in square brackets) is theoretical, computed assuming 3 fermion families,* $m_t < 100\ GeV$, *and* $M_H < 1\ TeV$. *In the other cases the theoretical and experimental uncertainties are combined. The quoted errors in* $\sin^2\theta_W$ *for the planned electroweak tests do not include uncertainties due to* m_t *and* M_H, *from [43], [44].*

ratio via

$$R_\nu = \sigma_\nu^{NC}/\sigma_\nu^{CC} = 1/2 - \sin^2\theta_W + 5/9\,\sin^4\theta_W\,(1+r) \qquad (Q^2 \ll M_Z^2) \tag{28}$$

The charged lepton-quark processes (μq and eq) are dominated by the electromagnetic (NC) photon exchange. Since the CC cross section is practically zero the weak-electromagnetic interference has been exploited. At BCDMS, where both $\mu^\pm$ beams with a polarization of $\lambda = 0.8$ were available, the mixed asymmetry $B(\lambda)$ could be used to extract $\sin^2\theta_W$ via:

$$B(\lambda) = \frac{\sigma_{NC}^+(\lambda) - \sigma_{NC}^-(\lambda)}{\sigma_{NC}^+(\lambda) + \sigma_{NC}^-(\lambda)} \propto (a_\mu - \lambda\, v_\mu) \qquad (Q^2 \ll M_Z^2) \tag{29}$$

At SLAC, where only a polarized electron beam ($\lambda = 0.37$) was available, the asymmetry A was measured:

$$A(\lambda) = \frac{\sigma_{NC}(\lambda) - \sigma_{NC}(-\lambda)}{\sigma_{NC}(\lambda) + \sigma_{NC}(-\lambda)} \propto \lambda[a_1(\theta_W) + a_2(\theta_W)\,Y_-/Y_+] \qquad (Q^2 \ll M_Z^2) \tag{30}$$

Clearly, the smallest statistical error can be gained in deep inelastic νN scattering, c.f. Table 3, it is even smaller than the theoretical uncertainties. The latter arise mostly from the charm quark threshold ($\Delta \sin^2\theta_W = 0.004$), the relative normalization of the antiquark-to-quark distributions ($\Delta \sin^2\theta_W = 0.002$), and higher twist contributions ($\Delta \sin^2\theta_W = 0.002$) [53].

The major advantage at HERA in testing the electroweak sector of the SM is clearly the large available Q^2 range. It not only allows scanning the electroweak parameters over a wide mass scale range but also to exploit the rise of the boson propagators with Q^2. Having both electron and positron beams as well as a longitudinal lepton polarization up to $\lambda = 80\%$ at hand and being able to measure NC and CC cross sections simultaneously each of the following quantities can be used for precision measurements at HERA: the differential cross sections $\tilde{\sigma}_{NC,CC}(e^\mp;\lambda)$, eqs. (12,16), the NC over CC cross section ratio, $R^\pm$, and various asymmetries like the pure NC asymmetry, $A^\pm$, and the charge asymmetry, B, defined by:

$$\begin{aligned} R^\pm(\lambda;x,Q^2) &= \frac{\tilde{\sigma}_{NC}^\pm(\lambda)}{\tilde{\sigma}_{CC}^\pm(\lambda)} \\ A^\pm(\lambda;x,Q^2) &= \frac{\tilde{\sigma}_{NC}^\pm(\lambda) - \tilde{\sigma}_{NC}^\pm(-\lambda)}{\tilde{\sigma}_{NC}^\pm(\lambda) + \tilde{\sigma}_{NC}^\pm(-\lambda)} \\ B(\lambda;x,Q^2) &= \frac{\tilde{\sigma}_{NC}^+(-\lambda) - \tilde{\sigma}_{NC}^-(\lambda)}{\tilde{\sigma}_{NC}^+(-\lambda) + \tilde{\sigma}_{NC}^-(\lambda)} \end{aligned} \tag{31}$$

A drawback of any ep collider like HERA in comparison with the fixed target lepton-quark-scattering experiments is the smaller statistics. In section 3 it was shown that about 500000 NC $e^\mp p$ but only 5000 (10000) CC $e^- p$ ($e^+ p$) events can be expected in a region where both the experimental systematic errors are small and the LL QCD description is valid. These numbers are to be contrasted with 500000 NC and CC events each in νN scattering experiments. An unavoidable problem when comparing cross section rates with theoretical predictions is caused by the uncertainty in the luminosity measurement which could hardly be less than 1% [4]. An improvement can be achieved by normalizing to the NC cross section at low Q^2 and then extracting the electroweak parameters at high Q^2. This method, however, relies heavily on the Q^2-evolution of the structure functions. The sensitivity to luminosity measurements as well as to further systematic errors like uncertainties in the quark densities can be reduced by analyses

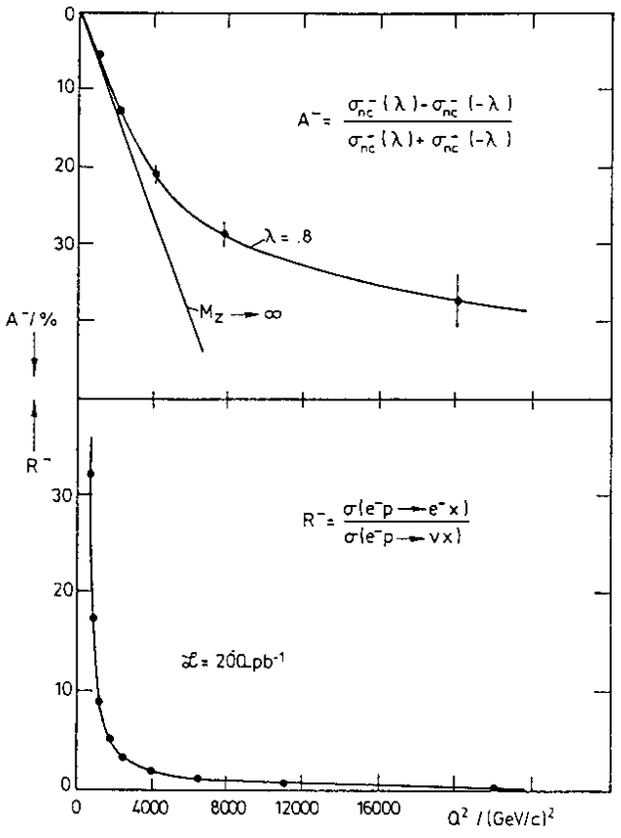

Figure 10: *Statistical precision of A^- and R^- at HERA for $\lambda = 0.8$ and $\sqrt{s} = 314\,GeV$ as a function of Q^2. The Monte Carlo results correspond to an integrated luminosity of 200 pb^{-1} which for A^- means 100 pb^{-1} per beam. From [57].*

of cross section ratios. The achievable experimental precision is then mainly limited by the available statistics.

The statistical precision of A and R in ep scattering at HERA with a longitudinal electron polarization of $\lambda = 0.8$ is shown in Figure 10 as a function of Q^2 [57]. The results of [57] are obtained using the parton density parametrization of [37] at maximum HERA energy $\sqrt{s} =$ 314 GeV and at 200 pb^{-1} which for A^- means 100 pb^{-1} per beam. Consider first the NC over CC cross section ratio R, eq. (31). The NC cross section at low Q^2 is dominated by photon exchange which falls off as $1/Q^4$ while at $Q^2 \geq M_Z^2$ the $\gamma - Z$ interference and the Z exchange contributions get larger. The CC cross section, on the other hand, depends only weakly on Q^2 and is of the same order as the Z exchange cross section. Thus R^- is large at low Q^2 and of order unity at high Q^2. Moreover, since the statistics is limited by the (smaller) CC cross section the statistical error is approximately constant over the whole Q^2 range. As a result the electroweak parameters can be extracted both at high and at low Q^2 with the same statistical error.

This is in contrast to the quantity A, eq. (31). The NC asymmetry vanishes at zero Q^2 and is of order 30% at high Q^2, see Figure 10. At low Q^2, A is proportional to Q^2:

$$A^-(\lambda) \sim -\lambda \frac{Q^2}{1 + Q^2/M_Z^2} \left(\frac{3}{2} - 4\sin^2\theta_W\right) \frac{\sqrt{2}G_F(1 - \Delta r)}{8\pi\alpha} \qquad (32)$$

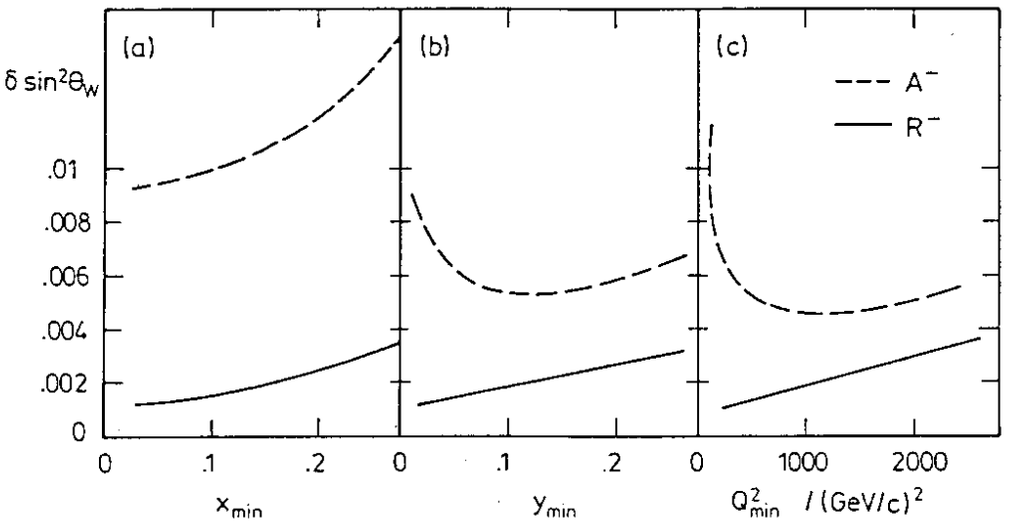

Figure 11: *Statistical error of* $\sin^2\theta_W$ *as a function of the lower limits on* x, y *and* Q^2 *at HERA. Further explanations are given in Fig. 10. From [57].*

Thus A is almost insensitive to M_Z for small Q^2, its slope coincides almost with the one for an infinitely heavy Z-boson. The sensitivity on the electroweak parameters of A increases with Q^2. But at the same time the statistical error on A increases, compare Figure 10. This is because both the cross sections of the numerator and the denominator of A become small with increasing Q^2. Thus there is a competition between sensitivity and statistics. The influence of the kinematical range chosen on the precision on $\sin^2\theta_W$ has been analyzed in [57] and is shown in Figure 11 where the $\pm 1\sigma$ statistical error of $\sin^2\theta_W$ is plotted against the lower limits in x, y and Q^2. The values of A at low Q^2 are almost insensitive to $\sin^2\theta_W$ and moreover have large statistical errors. Thus including Q^2 values below $\approx 500\,\mathrm{GeV}^2$ diminishes the accuracy on $\sin^2\theta_W$ when using A. Through the relation $Q^2 = xys$ it is clear that the same pattern is observed in the corresponding y distribution. It is thus sensible to restrict the ranges in y and Q^2 from below. Although extending the x-range to small values increases the cross section and improves the statistical error these regions should be excluded in order to reduce the uncertainties in the quark densities which are larger at low x. The results presented in the following in Table 4 and Figs. 12 and 13) are taken from [57]. The authors in [57] define a working area for the extraction of electroweak parameters from the measurement of A by $y > 0.01$, $Q^2 > 500\,\mathrm{GeV}^2$ and $x > 0.1$. From the statistical point of view the small kinematic parameter values should be included when using R^-. Yet, since the experimental reconstruction of DIS events should be restricted to the safe regions eq. (20) the working area for R^- was chosen to be same as for A where a slightly better result could be obtained by relaxing the cut on Q^2.

Apart from the top quark mass, m_t, and the Higgs mass, m_H, the SM is determined by three independent parameters which can be chosen from α, G_F, M_Z, M_W and $\sin^2\theta_W$ (assuming the ρ-parameter to be equal one). Fixing two of them the other parameters can be determined by comparing experimental and theoretical quantities (cross sections, etc.). The resulting sensitivity relies on the choice of parameters, i.e. when one changes the parametrization the sensitivity to the parameters changes also [3]. For example, the dependence on $\sin^2\theta_W$ of the CC propagator

[3] This is of course only true if the respective two input parameters are taken from different experiments.

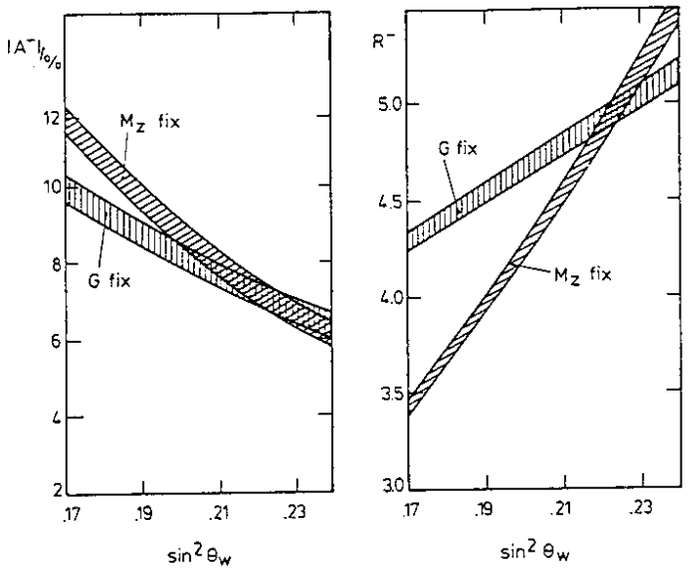

Figure 12: *A^- and R^- as functions of $\sin^2\theta_W$ for either (α, G_F) or (α, M_Z) fixed at HERA. The shaded areas correspond to $\pm 1\sigma$ statistical errors at $200\,pb^{-1}$, $\sqrt{s} = 314\,GeV$, and $\lambda = 0.8$. The included kinematical region is given by $y > 0.01$, $Q^2 > 500\,GeV^2$ and $x > 0.1$. From [57].*

and the NC interference term is illustrated in the following equations:
CC propagator:

$$\frac{\pi\alpha}{2\sin^2\theta_W}\,\frac{1}{Q^2+M_W^2} = \frac{G_F(1-\Delta r)}{\sqrt{2}}\,\frac{M_W^2}{Q^2+M_W^2} \tag{33}$$
$$= \frac{\alpha\pi}{2}\,\frac{1}{Q^2\sin^2\theta_W + A^2} = \frac{\alpha\pi}{2\sin^2\theta_W}\,\frac{1}{Q^2+M_Z^2\cos^2\theta_W}$$

NC interference term:

$$\frac{\pi\alpha^2}{Q^2x}\,\frac{1}{2\sin^2\theta_W\cos^2\theta_W}\,\frac{1}{Q^2+M_Z^2} = \frac{\alpha G_F(1-\Delta r)}{\sqrt{2}Q^2x}\,\frac{M_Z^2}{Q^2+M_Z^2} \tag{34}$$
$$= \frac{\alpha^2\pi}{2Q^2x}\,\frac{1}{A^2+Q^2\sin^2\theta_W\cos^2\theta_W}$$

where $A^2 = \pi\alpha/[G_F\sqrt{2}(1-\Delta r)]$. Δr takes into account one-loop electroweak corrections to the relation between M_Z, $\sin^2\theta_W$ and G_F. The sensitivity of A^- and R^- (at $\lambda = 0.8$) on $\sin^2\theta_W$ is shown in Figure 12 [57] for the two cases of fixing besides α either M_Z or G_F. The width of the dashed regions at constant $\sin^2\theta_W$ is given by $\pm 1\sigma$ statistical errors of the average A^- and R^-, respectively. It turns out that R^- is better suited than A^- to measure $\sin^2\theta_W$ and that fixing M_Z and not G_F results in the higher sensitivity. The χ^2 analysis of the sensitivity of A^- and R^- to a given electroweak parameter performed in [57] is summarized in Table 4. The best result is provided by the cross section ratio R^-, the statistical error being $\Delta\sin^2\theta_W = \pm 0.002$ if M_Z is fixed besides α. Taking G_F as the second input variable the error is larger, $\Delta\sin^2\theta_W = \pm 0.005$. Fixing M_Z instead of G_F still gives a better result even when taking into account the larger uncertainty of M_Z, see below. The error on M_W is e.g. 100 MeV for fixed M_Z. As expected from Figure 12 the results obtained from the NC asymmetry A^- are worse. While the NC

error on		fixed			
		$\sin^2\theta_W$	M_Z	M_W	G_F
$\sin^2\theta_W$	A^-		0.005	0.005	0.007
	R^-		0.002	0.002	0.005
M_Z	A^-	3.02		0.25	1.09
[GeV]	R^-	0.51		0.10	0.76
M_W	A^-	2.53	0.27		1.38
[GeV]	R^-	0.45	0.10		0.95

Table 4: *Statistical error of* $\sin^2\theta_W$, M_Z *and* M_W *in one-parameter fits assuming* α *and either* $\sin^2\theta_W$, M_Z, M_W *or* G_F *to be fixed. The upper values refer to* A^- *and the lower ones to* R^-. *Further explanations are given in Fig. 12. From [57].*

asymmetry A^- vanishes for zero polarization the cross section ratio R^- can still be used to extract the electroweak parameters. In fact, the statistical errors get only slightly worse when going from $\lambda = 0.8$ to $\lambda = 0$, by about 25% for M_W [57] and 15% for $\sin^2\theta_W$.

Several sources of uncertainties in the determination of electroweak parameters have to be considered. Besides the statistical errors, summarized in Table 4, there are systematical experimental uncertainties (section 3), uncertainties in the theoretical expressions and those coming from unknown input quantities. While systematic experimental uncertainties are of the order of the statistical errors when extracting electroweak parameters from cross section measurements [58], they are reduced by considering cross section ratios like $R^\pm$ and $A^\pm$, in particular when restricting the analysis to the safe regions, eq (20). Uncertainties in the theoretical expressions, i.e. effects of primordial $k_\perp$, higher twist contributions, thresholds from heavy quarks, higher order QCD corrections like a nonzero structure function F_L, etc., are small compared to the statistical error provided $Q^2 > 100\,\mathrm{GeV}^2$ and $x > 0.01$. For example, in [57] it was shown, that varying σ_L/σ_T from zero to 0.1 introduces an error on $\sin^2\theta_W$ which is about 0.3 (0.06) times smaller than the statistical error from R^- (A^-).

Determing one of the three independent electroweak parameters of the SM requires fixing of two other parameters (besides m_t and M_H). While α and G_F are known precisely, fixing M_Z or $\sin^2\theta_W$ may induce nonnegligible errors. In [57] it was found that the errors on $\sin^2\theta_W$ and M_W caused by a 50 MeV error on M_Z are negligible compared to the respective statistical errors. On the other hand, an error of 0.001 on $\sin^2\theta_W$ results in errors on M_Z and M_W of the order of their statistical errors. Further insufficiently known input quantities are the values of the CKM matrix elements and structure functions. The influence of the former is small since $m_c^2 \ll Q^2$, and σ_b and σ_t are negligible at high Q^2 ($\geq 100\,\mathrm{GeV}^2$). An attempt to estimate the influence of quark distribution uncertainties on the measured electroweak quantities was made in [57]. Two sources have to be considered, uncertainties in the relative normalizations (quark to antiquark, U/D, etc.), and insufficiently known shapes in x. By measuring quantities which do not depend on the electroweak parameters, like F_2 at low Q^2 or $\sigma_{CC}(e^+)/\sigma_{CC}(e^-)$, it seems

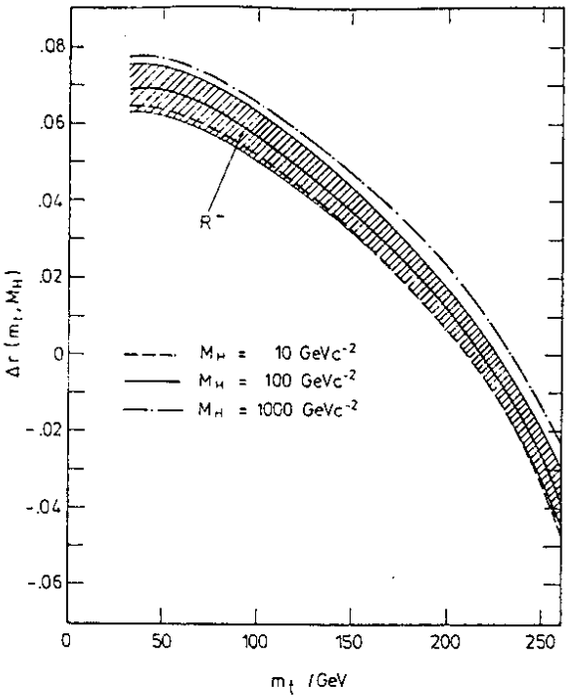

Figure 13: Δr *in dependence of* m_t *and* M_H. *The shaded area corresponds to the error induced for* Δr *by the* $\pm 1\sigma$ *statistical error of* R^- *taking* $M_H = 100$ *GeV. Further explanations are given in Fig. 12. From [57].*

possible to reduce the errors induced by structure functions to the order of the statistical errors. In general, uncertainties can be further reduced by comparing e.g. $\sin^2\theta_W$ obtained from A^-, R^- and R^+ and from measurements using different cuts on the kinematical variables.

In the direct channel the t-quark mass can be probed up to about 80 GeV at HERA [49]. Beyond this limit the top quark mass can still be constrained by studying the electroweak corrections. If α, G_F and $\sin^2\theta_W$ are taken as independent parameters, then the NC and CC Born (lowest order in α) electroweak cross sections are sensitive to the t quark and the Higgs boson masses, m_t and M_H, through the Δr term appearing in the CC propagator, eq. (33) and in the NC interference term, eq. (34) via

$$\begin{aligned} \Delta r &= \frac{\Sigma^W(0)}{M_W^2} + \frac{\alpha}{4\pi} c_1 \\ &= \frac{\alpha}{4\pi}\left[c_2 - c_3\, m_t^2/M_W^2 + c_1\right] \end{aligned} \tag{35}$$

The coefficients $c_i = c_i(\sin^2\theta_W)$ can e.g. be found in [14]. Fixing α, M_Z and G_F one can estimate the sensitivity of A^- and R^- to changes of Δr. This was investigated in [57,59]. For $m_t = 40$ GeV and $M_H = 100$ GeV the statistical error of Δr derived from A^- and R^- comes out to be 0.022 and 0.006, respsectively. Figure 13 illustrates the dependence of Δr on m_t and M_H. The dashed region indicates the $\pm 1\sigma$ deviation contour of $R^-(m_t)$ for $M_H = 100$ GeV. As can be seen, $[\Delta r(m_t, M_H = 10\,\text{GeV}) - \Delta r(m_t, M_H = 1000\,\text{GeV})]$ is larger than two standard deviations. This might be translated into a bound on M_H. Also, a constraint on m_t can probably be extracted. In particular with increasing t-quark mass a more precise measurement of m_t can be performed, e.g. for $m_t = 100$ GeV an error of ± 20 GeV seems feasible.

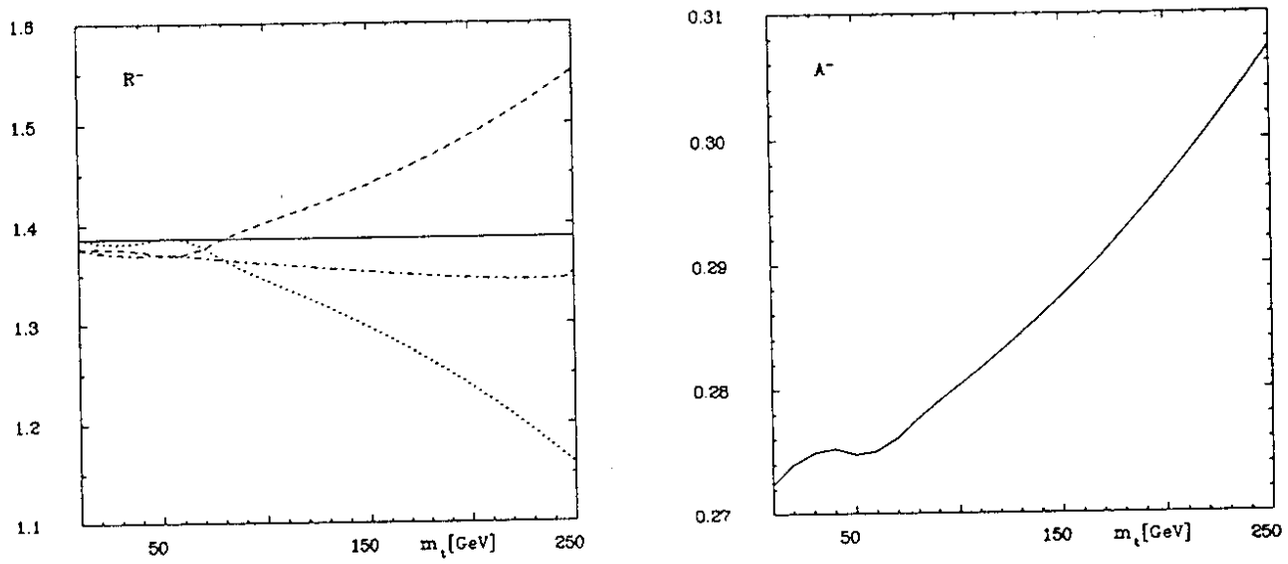

Figure 14: $R^-(x = y = 0.2)$ *and* $A^-(x = y = 0.3)$ *as functions of the top quark mass,* m_t*, at* $\sqrt{s} = 314\,GeV$*,* $\lambda = 1.0$*, and* $M_H = 100\,GeV$*. The one-loop calculation of* A^- *is shown for* (α, G_F, M_Z) *fixed. For* R^- *the one-loop calculation at fixed* (α, G_F, M_Z) *(dashed-dotted curve), the one-loop calculation at fixed* (α, M_W, M_Z) *(dashed curve), the Born calculation at fixed* (α, G_F, M_Z) *(dotted curve), and the Born calculation at fixed* (α, M_W, M_Z) *(soild curve). From [59].*

In the above analysis higher order electroweak corrections have not been included. These will modify the tree graph expressions eqs. (12, 16). While the corrections for cross sections can become large, cross section ratios are rather unaffected [14]. Important in this context is the fact that, at fixed M_Z and G_F, the CC propagator becomes practically independent of the t-quark mass. In the one-loop corrected expression for the W propagator

$$\frac{G_F}{\sqrt{2}} \frac{M_W^2}{Q^2 + M_W^2} \frac{1 - \Delta r}{1 - \Sigma^W(-Q^2)/(Q^2 + M_W^2)} \neq f(m_t) \tag{36}$$

Δr (eq. (35)) cancels almost completely against $-\Sigma^W(-Q^2)/(Q^2 + M_W^2)$. Thus $R^\pm$ is no longer sensitive to m_t for (M_Z, G_F) fixed, see Figure 14. The top mass dependence of the Born expression for R^- is also shown for comparison. Though the distributions are obtained for $x = y = 0.3$ it has been checked that the qualitative behaviour does not depend on the specific choice of the x, y values. In contrast, the cross section ratios $A^\pm$ still depend on m_t since the Δr term and the Z boson self energy do not completely cancel. At sufficiently low Q^2 and restricting to the dominating u quark contributions the following approximation holds [59]

$$A^-(\text{1-loop}) \sim A^-(\text{Born}) \left(1 + \frac{\alpha}{4\pi} \frac{m_t^2}{M_W^2} \frac{3}{4 \sin^2 \theta_W} + \delta_{\text{em+weak}}\right) \tag{37}$$

where $\delta_{\text{em+weak}}$ summarizes all other (small) corrections which do not depend on m_t. The top quark mass dependence of A^- at HERA is shown in Figure 14. Again the sensitivity on m_t is largely independent of the choice $x = y = 0.3$. The top mass dependence looks indeed rather promising. The question may be raised whether it is possible to obtain a steep top

mass dependence also in the one-loop corrected expression for R^-. The sensitivity of R^- to m_t can in fact be increased by fixing M_Z and M_W instead of M_Z and G_F. The result is shown in Figure 14. As can be seen the top mass dependence of the one-loop corrected expression of R^- at fixed M_Z and M_W is quite the same as the corresponding dependence of the Born expression when M_Z and G_F are fixed. But the larger experimental uncertainty on M_W has to be taken into account which will probably compensate the larger sensitivity to m_t. In conclusion it seems feasible to determine m_t through radiative corrections at HERA, most likely through measurements of A^-.

9 Conclusions

Physics opportunities at the ep collider HERA have been reviewed. It has been stressed that there is a wide variety of physics at low Q^2 besides the more standard physics in deep inelastic scattering. The general formula valid for all hard processes at HERA has been given explaining how it can be applied to the description of the various modes of HERA. These modes are naturally divided into the deep inelastic mode and those mediated by the exchange of an almost real photon. The latter processes proceed at low Q^2 and include contributions coming from the pointlike couplings of the photon to the partons in the proton, the anomalous photon component, the VDM component, and from diffractive reactions. Through forward electron detectors precision measurements can also be performed in photoproduction. Prospects are production of heavy objects (heavy quarks, weak bosons, new particles, etc.), prompt photon and lepton pair production, hard diffractive reactions, measurements of the proton's structure function, and explorations of the anomalous photon structure function, in particular of its gluonic component which is not directly accessible in $\gamma\gamma^*$ experiments.

Experimentation at HERA will also help to clarify many phenomena at the boundary between perturbative and nonperturbative effects. A few topics are final state hadronization of both the quark and proton remnant jets, coherent and higher twist contributions to lepton-nucleon scattering at low Q^2, Regge behaviour in non-singlet structure functions, jet coalescence, and (quasi-) elastic scatterings. The forward proton detector will be useful for these classes of events.

The deep inelastic mode is best suited for precison tests of the SM. The prospects in determing the x shape of structure functions and quark momentum distributions, extracting the gluon density and testing QCD scaling violations, as well as measuring electroweak parameters at HERA have been discussed. The relevant measurements are obtained from inclusive NC and CC cross sections for electron and positron-proton scattering. Experimental limitations of the accessible kinematical region in x and y (or Q^2) should be kept as small as possible since they will diminish the physics potential of HERA. An additional run of HERA at a lower cms energy will improve its physics capacity, like the prospects of measuring the gluon density, determing Λ_{QCD}, or bridging a possible gap between structure function measurements possible at HERA and existing measurements at fixed target experiments.

On the theoretical side, the unknown low x behaviour of structure functions causes further constraints. In order to use the LL approximation of QCD one usually restricts the analysis to $x > 0.01$ and looses thus the high statistics expected at very low x. On the other hand, HERA might enter the region where $\ln(1/x)$ terms become important. More theoretical work is needed to exploit this challenging aspect of QCD, in particular since with e.g. F_2^{em} there are sensitive probes of low x physics which are well measurable down to $x \sim 10^{-4}$.

In conclusion, HERA offers a rich physics program. A (incomplete) list of topics is: Investigation of the proton structure, in particular at high Q^2 and low x, and of the hadronic nature of the photon, extraction of quark and gluon momentum distributions of both the proton and the photon, studies of scaling violations of DIS structure functions in a large range of Q^2, tests of perturbative QCD in hard scattering processes and exploration of many nonperturbative effects, examination of the structure of weak and charged weak currents, Z and W propagators within and beyond the SM, electroweak radiative effects, charm, bottom and top quark physics and last not least searches for new physics. The direct way leptons probe the nucleon structure together with the large Q^2 range make HERA complementary to other machines.

Acknowledgements. I am grateful to J. Blümlein, G. Ingelman, G. Kramer, H. Spiesberger and G. Wolf for fruitful discussions. I thank G. Bellettini and M. Greco for organizing an interesting workshop and a pleasant stay in La Thuile.

References

[1] HERA – a proposal for a large electron-proton colliding beam facility, DESY/HERA 81/10 (1981).

[2] H1 Collaboration, Technical Proposal for the H1 detector (1986); ZEUS Collaboration, Technical Proposal for the ZEUS detector (1986).

[3] B. Diekmann et al., Proc. of the HERA Workshop, Hamburg, 1987, Ed. R.D. Peccei, p. 515.

[4] L. Suszycki et al., Proc. of the HERA Workshop, Hamburg, 1987, Ed. R.D. Peccei, p. 505.

[5] G. Ingelman and G.A. Schuler, Z. Phys. C40 (1988) 299.

[6] P. Aurenche et al., Nucl. Phys. B286 (1987) 553.

[7] G. Ingelman and P. Schlein, Phys. Lett. B152 (1985) 256.

[8] K. H. Streng, Proc. of the HERA Workshop, Hamburg, 1987, Ed. R.D. Peccei, p. 365.

[9] S. J. Brodsky, J. F. Gunion and D. E. Soper, Phys. Rev. D36 (1987) 2710.

[10] S. J. Brodsky, C. Person and N. Sakai, Phys. Rev. D23 (1981) 2745; S. J. Brodsky, P. Hoyer, C. Person and N. Sakai, Phys. Lett. 93B (1980) 451.

[11] M. Glück, R.M. Godbole and E. Reya, Z. Phys. C38 (1988) 441.

[12] G. Altarelli and G. Parisi, Nucl. Phys. B126 (1977) 298; G. Altarelli, Phys. Rep. 81 (1982) 1.

[13] J.G. Körner, E. Mirkes and G.A. Schuler, Mod. Phys. A4 (1989) 1781.

[14] For discussions of radiative corrections in deep inelastic scattering and references to original papers, see e.g. W. Hollik, Proc. of the HERA Workshop, Hamburg, 1987, Ed. R.D. Peccei, p. 579; H. Spiesberger, *ibid*, p. 605; J. Kripfganz and H. Perlt, *ibid*, p. 645; C. Kiesling, *ibid*, p. 653.

[15] J. Blümlein, M. Klein, T. Naumann and T. Riemann, Proc. of the HERA Workshop, Hamburg, 1987, Ed. R.D. Peccei, p. 67; J. Blümlein, M. Klein and T. Naumann, Berlin preprint PHE 88-12 and to appear in 'New Theories in Physics', Proc. Int. Conf. High Energy Physics, Kazimierz, Poland, 1988, Ed. Z. Adjuk, (World Scientific, Singapore).

[16] J. Blümlein, G. Ingelman, M. Klein and R. Rückl, in preparation.

[17] G. Ingelman, D. Notz and E. Ros, Proc. of the HERA Workshop, Hamburg, 1987, Ed. R.D. Peccei, p. 19.

[18] J. Feltesse, Proc. of the HERA Workshop, Hamburg, 1987, Ed. R.D. Peccei, p. 33.

[19] L.V. Gribov, E.M. Levin and M.G. Ryskin, Phys. Rep. 100 (1983) 1.

[20] G. Ingelman and R. Rückl, Proc. of the HERA Workshop, Hamburg, 1987, Ed. R.D. Peccei, p. 107.

[21] G. Ingelman and R. Rückl, DESY 89-023 (1989).

[22] G. Ingelman and R. Rückl, Phys. Lett. 201B (1988) 369.

[23] E. Eichten, I. Hinchliffe, K. Lane and C. Quigg, Rev. Mod. Phys. 56 (1984) 579; ibid. 58 (1986) 1047.

[24] D. Allasia et al., WA25 Collaboration, Z. Phys. C28 (1985) 321.

[25] H. Abramowicz et al., CDHS Collaboration, Z. Phys. C25 (1984) 29.

[26] J.J. Aubert et al., EMC Collaboration, Nucl. Phys. B259 (1985) 189.

[27] A.D. Martin, R.G. Roberts and W.J. Stirling, Phys. Rev. D37 (1988) 1161.

[28] A. M. Cooper-Sarkar, G. Ingelman, K. R. Long, R. G. Roberts and D. H. Saxon, Z. Phys. C39(1988) 281.

[29] S. M. Traczyk, W. J. Stirling and D. H. Saxon, Proc. of the HERA Workshop, Hamburg, 1987, Ed. R.D. Peccei, p. 265.

[30] Z. Kunszt, Phys. Lett. B207 (1988) 103.

[31] A. D. Martin, C.-K. Ng and W. J. Stirling, Phys. Lett. B191 (1987) 200.

[32] G. Barbagli and G. D'Agostini, Proc. of the HERA Workshop, Hamburg, 1987, Ed. R.D. Peccei, p. 135.

[33] J. Kwiecinski, Z. Phys. C29 (1985) 561.

[34] A. Bodek at al., SLAC-MIT collaboration, Phys. Rev. D20 (1979) 1471.

[35] A. C. Benvenuti et al., BCDMS collaboration, paper No. 218 subm. to the 1987 Symp. on Lepton and Photon interactions at High Energies, Hamburg, Germany, 27–31 July 1987.

[36] W. Furmanski and R. Petronzio, Nucl. Phys. B195 (1982) 237.

[37] D.W. Duke and J.F. Owens, Phys. Rev. D30 (1984) 49.

[38] K. J. F. Gaemers, R. M. Godbole and M. van der Horst, Proc. of the HERA Workshop, Hamburg, 1987, Ed. R.D. Peccei, p. 739.

[39] M. Böhm and A. Rosado, Z. Phys. C39 (1988) 275.

[40] D. Atwood et al., CERN-TH-5213/88 (1988).

[41] See F. Cornet and R. Rückl, Proc. of the HERA Workshop, Hamburg, 1987, Ed. R.D. Peccei, p. 771, and the references therein.

[42] J. Bijnens, Proc. of the HERA Workshop, Hamburg, 1987, Ed. R.D. Peccei, p. 819; N. Harnew, ibid. p. 829; Ch. Berger et al., ibid. p. 851.

[43] K. Hagiwara, S. Komamiya and D. Zeppenfeld, Z. Phys. C29 (1985) 115.

[44] Ch. Berger et al., Proc. of the HERA Workshop, Hamburg, 1987, Ed. R.D. Peccei, p. 813.

[45] J. Bartels, Proc. of the HERA Workshop, Hamburg, 1987, Ed. R.D. Peccei, p. 863; L. Stanco, ibid. p. 889.

[46] R. Rückl, Phys. Lett. 129B (1983) 363; Nucl. Phys. B234 (1984) 91.

[47] H.-U. Martyn, Proc. of the HERA Workshop, Hamburg, 1987, Ed. R.D. Peccei, p. 801 and references therein.

[48] W. Buchmüller, B. Lampe and N. Vlachos, Phys. Lett. 197B (1987) 379.

[49] G. Ingelman, G. A. Schuler and J. F. de Trocóniz, Nucl. Phys. B317 (1989) 1.

[50] G. A. Schuler, Nucl. Phys. B299 (1988) 21; U. Baur and J.J. van der Bij, Nucl. Phys. B304 (1988) 451; R.A. Eichler and Z. Kunszt. Nucl. Phys. B308 (1988)791.

[51] G. A. Schuler, DESY 89-018 (1989) and to appear in Proc. of the 5^{th} workshop of the INFN Eloisatron Project, Erice, Italy 1988, Editor: A. Ali.

[52] R.K. Ellis and P.Nason, Nucl. Phys. B312 (1989) 551.

[53] U. Amaldi et al., Phys. Rev. D36 (1987) 1385.

[54] R. Marshall, Rutherford RAL-88-051 (1988).

[55] See Physics at LEP, CERN (1986), Eds. J. Ellis and R.D. Peccei.

[56] P. Langacker, Penn U. (1988), Print-88-0767.

[57] J. Blümlein, M. Klein and T. Riemann, PHE-87-03 (1987), published in Warsaw Sympos. 1987:39; also in Proc. of the HERA Workshop, Hamburg, 1987, Ed. R.D. Peccei, p. 687.

[58] O. Gry, G. D. Heath and E. Paul, Proc. of the HERA Workshop, Hamburg, 1987, Ed. R.D. Peccei, p. 719.

[59] G. A. Schuler and H. Spiesberger, in preparation.